The Effect of STAT5 on Inflammation-Related Gene Expression in Diabetic Mouse Kidneys

A thesis presented to

the faculty of

the College of Arts and Sciences of Ohio University

In partial fulfillment

of the requirements for the degree

Master of Science

Samantha J. Shaw

May 2014

This thesis titled

The Effect of STAT5 on Inflammation-Related Gene Expression in Diabetic Mouse Kidneys

by

SAMANTHA J. SHAW

has been approved for

the Department of Biological Sciences

and the College of Arts and Sciences by

Karen T. Coschigano

Associate Professor of Biomedical Sciences

Robert Frank

Dean, College of Arts and Sciences

ABSTRACT

SHAW, SAMANTHA J., M.S., May 2014, Biological Sciences

The Effect of STAT5 on Inflammation-Related Gene Expression in Diabetic Mouse Kidneys

Director of Thesis: Karen T. Coschigano

Diabetic nephropathy (DN) is the leading cause of end-stage renal disease and renal failure in humans. The molecular pathways that lead to DN are not well known. This research investigates possible roles of several signal transducers and activators of transcription (STAT) proteins in this disease using a STAT5A/B knockout (SKO) mouse model. Based on previous observations of increased inflammation-related gene expression in the kidneys of diabetic SKO mice, the hypothesis of the current project was that the combination of the loss of STAT5 repression and increase of STAT3 activity escalates inflammation-related gene expression in the kidneys of diabetic SKO mice. In support of this hypothesis, an increase of IRF-1 RNA expression, reflective of the loss of STAT5 repression, was observed in the kidneys of diabetic SKO mice. Levels of phosphorylated STAT3 were also increased in the kidneys of diabetic SKO mice. These results suggest that STAT5 acts as a repressor of inflammation-related genes in DN and, in its absence, expression of these genes is no longer repressed, either due to direct loss of the STAT5 repression or due to increased STAT3 activity which could potentially increase their expression.

DEDICATION

I would like to dedicate my thesis to my late Grandmother, Virginia Weston, who was always proud of me, believed in me, shared her faith, and to whom I attribute my curiosity.

ACKNOWLEDGMENTS

First and foremost I would like to thank my mentor, Dr. Karen Coschigano, for her support, encouragement, and guidance in my research. Without her this thesis would not have been possible. I would also like to thank Dr. Masato Nakazawa for all the time and energy spent on guiding me through the statistics for my data. I would also like to thank my committee members, Dr. Calvin James and Dr. Ramiro Malgor, for their time, support, and patience through this process. I would also like to thank Dr. Lonnie Welch for his encouragement and teaching me the basics of Bioinformatics; I would not have the alignments in my thesis if it were not for him. I would also like to thank the members, past and present, of Dr. Karen Coschigano's lab, for all their help, support, and previous results. Lastly I would like to thank God, who was there through it all.

TABLE OF CONTENTS

Page

LIST OF TABLES

Page

LIST OF FIGURES

Page

CHAPTER 1: INTRODUCTION

1.1 Diabetes

The American Center for Disease Control states that 8.3% of the American population, or 25.8 million people, have type 1 or type 2 diabetes and that 1.9 million cases of diabetes were diagnosed in 2010 for people aged 20 years and older (Centers for Disease Control and Prevention, 2011). Diabetes mellitus is characterized by hyperglycemia caused by defects in insulin secretion and/or insulin action (American Diabetes Association, 2012). The symptoms for diabetes include excessive thirst, hunger, and urination (van Belle, Coppieters, & von Herrath, 2011). There are two broad etiopathogenic classes: type 1 diabetes and type 2 diabetes (American Diabetes Association, 2012). There are also other types of diabetes, such as gestational diabetes, diseases of the exocrine pancreas, and diabetes from genetic defects of β-cell and insulin action (American Diabetes Association, 2012).

Type 1 diabetes makes up 5-10 percent of diabetic cases (American Diabetes Association, 2012). It is caused by an absolute deficiency of insulin secretion caused by cell-mediated autoimmune β-cell destruction in the pancreas (American Diabetes Association, 2012; Atkinson & Skyler, 2012; van Belle et al., 2011). There are multiple genetic predispositions for the autoimmune destruction of β-cells, such as mutations in the genes that encode human leukocyte antigens (HLA) (American Diabetes Association, 2012; Atkinson & Skyler, 2012). There are also environmental factors that are related to the destruction of β-cells, such as viral and bacterial infection, but they are poorly defined (American Diabetes Association, 2012; van Belle et al., 2011).

In Type 1 diabetes the rate of β-cell destruction is variable, from rapid (typically occurring in infants and children) to slow (typically occurring in adults) (American Diabetes Association, 2012). In some patients, especially children and adolescents, first manifestation of the disease may present as ketoacidosis. Ketoacidosis occurs when cells use fat as an alternative fuel to glucose (American Diabetes Association, 2014). This causes a buildup of the byproduct ketoacids. Modest fasting hyperglycemia in other

patients quickly turns into severe hyperglycemia and/or ketoacidosis with the presence of infection or other stress (American Diabetes Association, 2012). Residual β-cell function may be retained in other patients, in particular, adults, preventing ketoacidosis for many years. These patients will eventually be at risk for ketoacidosis and will require insulin to survive. Immune-mediated diabetes typically occurs in adolescence and childhood but can occur at any age, even in a person's 80's and 90's.

Type 2 diabetes makes up ~90-95 percent of diabetic cases (American Diabetes Association, 2012). Patients with type 2 diabetes have a resistance to insulin. These patients initially exhibit a rise in insulin levels as the tissues become resistant to insulin's effect. Eventually the elevated insulin levels are actually lower than expected as these patients develop an insulin secretion defect such that insulin secretion is not sufficient to compensate for the insulin resistance. Type 2 diabetic patients usually do not require insulin treatment for survival, at least at initial diagnosis. Most patients who are type 2 diabetic are obese; those who are not obese by typical weight criteria tend to have a higher percentage of fat distribution in the abdominal region. Obesity itself causes insulin resistance to some degree. Autoimmune β-cell destruction does not occur in type II diabetes. Ketoacidosis rarely occurs in these patients; if it does, it is typically connected with the stress of another illness. Genetics for type 2 diabetes are complex and not well defined, but there is a strong genetic predisposition association, more so than for the autoimmune type 1 diabetes.

Chronic hyperglycemia causes long term complications (American Diabetes Association, 2012). These include nephropathy ending in renal failure; retinopathy possibly leading to vision loss; peripheral neuropathy with the threat of Charcot joints, foot ulcers, and amputations; and autonomic neuropathy that causes sexual dysfunction and genitourinary, gastrointestinal, and cardiovascular symptoms. Increased occurrence of atherosclerotic, cardiovascular, cerebrovascular, and peripheral arterial diseases are also found in patients with diabetes. People with diabetes often have abnormalities of lipoprotein metabolism and hypertension as well. This research focuses on nephropathy in Type 1 diabetes.

1.2 Diabetic Nephropathy

The kidneys are a pair of bean-shaped organs that are located next to the posterior wall in the abdominal cavity (Eroschenko, 2008). They are covered in an irregular connective tissue called the renal capsule. Within the kidney are two regions, the outer cortex and the inner medulla (Eroschenko, 2008). The cortex contains the functional units of the kidney which are the uriniferous tubules (Eroschenko, 2008). Each unit is composed of two parts, the nephron and the collecting duct (Fig. 1). The nephron is made up of a renal corpuscle and renal tubule. Within the renal corpuscle there is a cluster of capillaries called the glomerulus (Fig. 1). The glomerulus is surrounded by the Bowman's capsule, which is a double layer of epithelial cells.

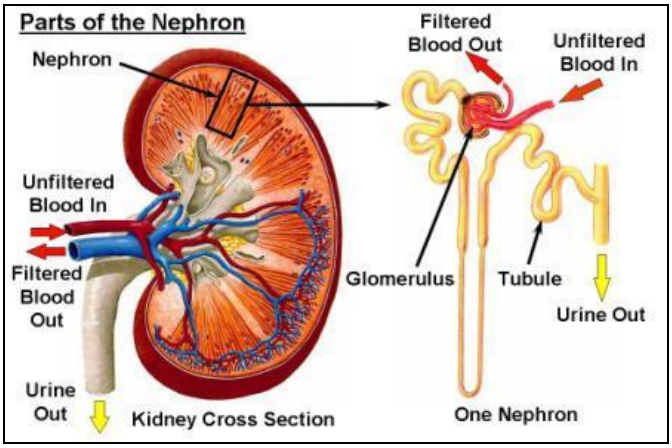

Figure 1. Kidney Diagram. Source: www.unckidneycenter.org. Used with permission.

The kidneys are vital for maintenance of whole body homeostasis (Eroschenko, 2008). The kidneys perform three main functions: blood filtration in the glomeruli, reabsorption of nutrients and other needed substances in the tubules, and secretion or excretion of unwanted substances or metabolic waste products in the filtrate (Fig. 1) (Eroschenko, 2008). The filtrate then enters the bladder and exits as urine (Eroschenko, 2008).

One of the major micro-vascular complications of diabetes is diabetic nephropathy (DN) (Kanwar et al., 2008; Luis-Rodriguez, Martinez-Castelao, Gorriz, De-

Alvaro, & Navarro-Gonzalez, 2012). DN is now the leading cause of end-stage renal disease and renal failure in humans (Luis-Rodriguez et al., 2012; Navarro-Gonzalez, Mora-Fernandez, Muros de Fuentes, & Garcia-Perez, 2011). Pathophysiologic changes of the kidney caused by diabetes include microalbuminuria and hyperfiltration (Kanwar et al., 2008). Renal functions worsen in association with cellular and extracellular derangements in the tubulointerstitial and glomerular compartments (Kanwar et al., 2008). DN is characterized by increased production of mesangial matrix and thickening of the glomerular and tubular basement membranes, and eventually tubulointerstitial fibrosis and glomerulosclerosis (Fig. 2) (Kanwar et al., 2008; Tervaert et al., 2010). Increased tubulointerstitial fibrosis can be caused by a variety of mechanisms, such as profibrotic and proinflammatory responses in proximal tubular cells that are triggered by endocytosis and albumin binding (Brosius, 2008). Glomerulosclerosis may be initiated by extraglomerular cells, such as macrophages and bone marrow-derived mesangial cell progenitors (Brosius, 2008; Tervaert et al., 2010).

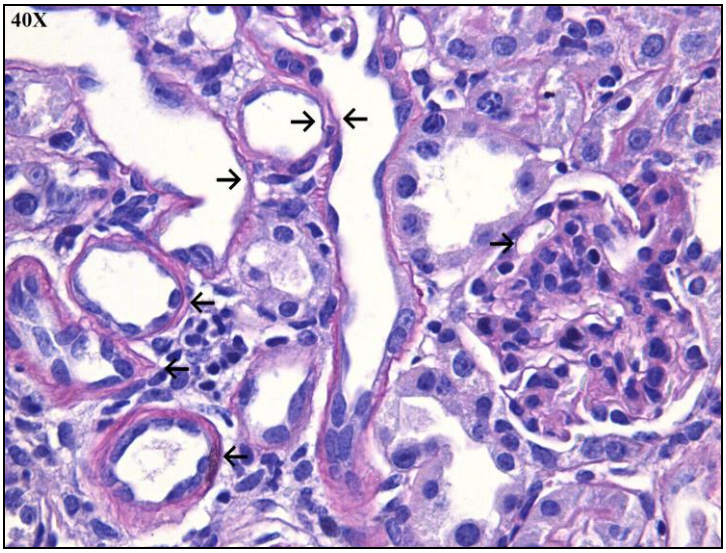

Figure 2. Periodic acid-Schiff (PAS) stained formalin-fixed, paraffin-embedded mouse kidney section. Arrows indicate examples of basement membrane thickening.

It was once thought that DN was caused by the interactions between metabolic and hemodynamic factors, but it is now known that inflammation is a key pathophysiological mechanism for DN (Navarro-Gonzalez et al., 2011). Recent studies

suggest that inflammatory pathways are major players in the development of diabetic complications like DN (Navarro-Gonzalez et al., 2011). It is known that an activated innate immunity, with chronic low-grade inflammation, contributes to the pathogenesis of diabetic nephropathy (Luis-Rodriguez et al., 2012). What is not well known are the molecular pathways that lead to this disease (Luis-Rodriguez et al., 2012). Defining these pathways is important as they have the possibility to serve as new drug targets (Luis-Rodriguez et al., 2012; Navarro-Gonzalez et al., 2011).

1.3 STAT Family

Many of the signal transducers and activators of transcription (STAT) transcription factors have a role in acquired and innate immunity (Teglund et al., 1998). There are seven mammalian STAT family members (STAT1, 2, 3, 4, 5a, 5b, and 6), located in three chromosomal regions (Ihle, 2001; Matsui & Meldrum, 2012; Teglund et al., 1998; Yu-Lee, 2001). A common core structure is shared by all STAT proteins (Buitenhuis, Coffer, & Koenderman, 2004; Jamieson, Farlik, & Decker, 2012). The amino-terminal region contains a series of eight short interactive helices and has been implicated in playing a role in the association of two separate STAT dimers that are bound to adjacent STAT DNA consensus sequences; this tetramer formation is required for optimal transcriptional activation (Buitenhuis et al., 2004). Located in the center of the protein is the DNA-binding domain that consists of several β-sheets (Buitenhuis et al., 2004). All except STAT2 have this DNA-binding domain; STAT2 uses the DNA-binding domains from its associated proteins (Jamieson et al., 2012; Yu-Lee, 2001). A classic Src homology (SH2) domain is necessary for STAT dimerization and for intracellular recruitment to cell surface receptors (Buitenhuis et al., 2004; Jamieson et al., 2012; Yu-Lee, 2001). After the SH2 domain is the C-terminal transactivation domain, which interacts with transcriptional coactivator proteins (Buitenhuis et al., 2004; Paulson et al., 1999). Other functional domains include a coiled-coiled domain, linker domain, and the critical tyrosine residue which is vital for dimerization, translocation into the nucleus and DNA binding (Yu-Lee, 2001).

Isoforms exist for most members of the STAT family (Jamieson et al., 2012). STATs either go through alternative mRNA splicing or a post-translational proteolytic process to form different isoforms (Lim & Cao, 2006). The alpha isoform is the full length STAT and the beta isoform is the smaller protein that usually lacks part of or the entire C-terminal transactivation domain (Jamieson et al., 2012; Lim & Cao, 2006). The shorter isoforms of STAT3 and STAT4 have specific sets of genes that they activate. It is not well understood how the α and β isoforms of STATs identify different sets of target genes.

STATs are activated by hormones, growth factors, and many cytokines, including interleukins (IL) and interferons (Lim & Cao, 2006; Matsui & Meldrum, 2012). The activators bind receptors, which undergo conformational changes that activate an associated Janus Kinase (JAK) (Fig. 3) (Jamieson et al., 2012; Lim & Cao, 2006). JAK then trans-phosphorylates the receptor's intracellular domain creating the docking sites for the STATs. Bound STAT is phosphorylated at a specific tyrosine residue on its cytoplasmic tail (Hennighausen & Robinson, 2008; Lim & Cao, 2006; Teglund et al., 1998). This leads to hetero- or homodimerization of the STATs by reciprocal binding of the phosphorylated tyrosines and translocation into the nucleus (Jamieson et al., 2012; Lim & Cao, 2006).

Upon activation and translocation to the nucleus, STATs bind specific DNA binding elements and activate transcription (Fig. 3) (Lim & Cao, 2006). Binding elements recognized by STATs contain consensus sequences such as gamma interferon-activated site (GAS) (Hennighausen & Robinson, 2008; Jamieson et al., 2012; Lim & Cao, 2006). The GAS consensus sequence is a small palindrome, $TTCN_XGAA$ (Jamieson et al., 2012). Variant sequences of GAS, $TTAN_3TAA$ or $TTCN_3TAA$, are known to be functional STAT binding sites as well. A DNA-dependent tetramerization of adjacent STAT dimers is essential for activation of a significant number of target promoters (Jamieson et al., 2012). This tetramerization is created through an N-terminal mediated interaction of the adjacent STAT dimers.

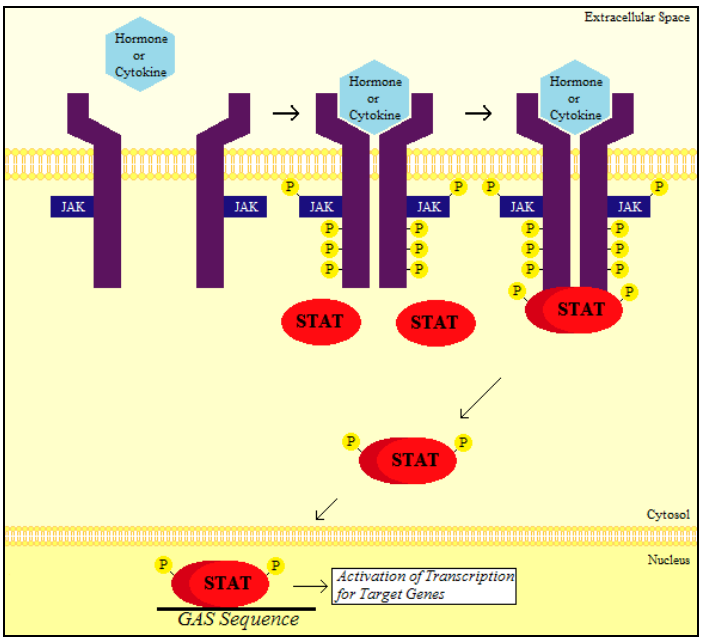

Figure 3. JAK/STAT Pathway. General scheme of STAT activation by hormones or cytokines through JAK.

STAT activation can be regulated through posttranslational modification (Jamieson et al., 2012). Posttranslational modification includes sumoylation of a lysine residue in the vicinity of the phosphorylated tyrosine; for some STATs this can inhibit transcriptional activity (Jamieson et al., 2012; Lim & Cao, 2006). The ability of DNA-bound STAT to contact the transcriptional machinery can be prevented by phosphorylation of the C-terminal serine (Jamieson et al., 2012). STAT1 and STAT3 have Serine727 located in their transactivation domain, with similar locations for STATs 4, 5, and 6. STAT activation is also regulated through abundance (Jamieson et al., 2012). Cytokines increase their own signals by increasing the amount of STATs. Sensitivity to a cytokine can be adjusted by lowering the amount of STAT proteins expressed in a cell.

STATs are predominantly known as transcriptional activators, but several gene expression profiles from STAT-deficient cells show a repressive role of STATs and the genes to which they bind (Jamieson et al., 2012). An example of this is STAT5 suppression of the interferon regulatory factor (IRF) 8 gene in response to granulocyte-macrophage colony-stimulating factor (GM-CSF) treatment of bone marrow-derived dendritic cell progenitor cells to repress their plasmacytoid development.

1.4 STAT5A/B

STAT5A and STAT5B are two highly related proteins in the STAT family (Hennighausen & Robinson, 2008; Ihle, 2001). The two genes that encode these proteins are located on chromosome 11 in mice (Hennighausen & Robinson, 2008; Lim & Cao, 2006; Teglund et al., 1998). The genes are juxtaposed and transcription starts within 10 kb of each other (Hennighausen & Robinson, 2008).

The STAT5 proteins are equally distributed in many tissues, but STAT5A is more prevalent in mammary tissue, while STAT5B is more prevalent in liver and muscle (Hennighausen & Robinson, 2008). The two proteins show a 96% sequence similarity (Liu, Robinson, Gouilleux, Groner, & Hennighausen, 1995). The two proteins have only one main difference and that is in their C-terminal region, which contains a transcriptional activator sequence (Liu et al., 1997). The STAT5B protein has 8 amino acids in the C-terminus that are completely diverged from those in STAT5A (Liu et al., 1995). Also, STAT5B is shorter than STAT5A by 12 amino acids in the C-terminal region (Liu et al., 1995).

STAT5A and STAT5B can be activated by growth hormone (GH), prolactin (PRL), epidermal growth factor (EGF), erythropoietin (EPO), interleukins and many different cytokines (Liu et al., 1997; Udy et al., 1997). PRL acts mainly through STAT5A and GH acts mainly though STAT5B (Cui et al., 2004; Liu et al., 1997; Udy et al., 1997). Activation of the STAT5A and STAT5B proteins occurs by ligand activation of JAK that in turn phosphorylates STAT5A and STAT5B on the tyrosine residues Y694 and Y699, respectively (Buitenhuis et al., 2004). STAT5A and STAT5B then form homo- or hetero-dimers and translocate into the nucleus for the transcriptional activation of a variety of genes (Buitenhuis et al., 2004). STAT5A can also be phosphorylated on Ser779 by p21-activated kinases which induce the β-casein promoter activity (Buitenhuis et al., 2004).

Disruption of STAT5A or STAT5B genes, either separately or together, revealed unique and redundant roles for these two proteins (Buitenhuis et al., 2004; Cui et al., 2004). The unique roles of these two related proteins are probably due to the differences in the C-terminal region as described above (Buitenhuis et al., 2004). STAT5A deficient

mice have a loss of PRL-dependent mammary development, the epithelium cannot differentiate during pregnancy, and the mice fail to lactate (Cui et al., 2004; Liu et al., 1997). Mammary development and function is not adversely effected in STAT5B deficient mice (Cui et al., 2004). STAT5B mediates the GH effects of sexual dimorphism of body growth rates and liver gene expression for which STAT5A is not able to substitute (Udy et al., 1997). When both STAT5A and STAT5B are deficient, there is a severe compromise in T-cell proliferation, the mammary alveolar epithelium fails to proliferate and differentiate during pregnancy, and ovarian development is altered (Cui et al., 2004; Teglund et al., 1998).

Little is known regarding the down-regulation of STAT5 protein activity, although several pathways have been shown to play a role (Buitenhuis et al., 2004). The C-terminal transactivation domain of STAT5A and STAT5B is required for the down-regulation of phosphorylated STAT5A and STAT5B in a proteasome-dependent way. Nuclear and cytoplasmic phosphatases dephosphorylate the STAT5 proteins. A negative feedback loop is seen for transcriptional activation of the suppressors of cytokine signaling (SOCS) family members by STAT5 proteins; the SOCS proteins inhibit the STAT5 proteins by association with the phosphorylated cytokine receptors or with the JAK proteins, preventing catalytic activity.

Two types of STAT5 knockout mice have been created. The first were genetically engineered to have a deletion in the first coding exon of the STAT5A and STAT5B genes (Teglund et al., 1998). These mice express STAT5A and STAT5B proteins with truncated N-termini; therefore, they can form dimers but not tetramers (Hennighausen & Robinson, 2008). Truncated protein is detected at 1% or less of the normal protein levels (Teglund et al., 1998). This makes them hypomorphic for STAT5A and STAT5B (Hennighausen & Robinson, 2008; Teglund et al., 1998). These mice are smaller than wild type mice, are severely compromised in T-cell proliferation, and the females are infertile (Cui et al., 2004; Hennighausen & Robinson, 2008; Teglund et al., 1998). These are the mice that were studied in this thesis. The second knockout mouse completely lacks the *STAT5A* and *STAT5B* loci (Cui et al., 2004). To create these mice, Cre-

expressing transgenic lines were used to delete the *loxP* bracketed 110-kb *STAT5* locus. These mice exhibit perinatal lethality.

1.5 STAT3

In the absence of STAT5, an increase of phosphorylated STAT3 in hepatocytes and liver tissue has been observed (Cui et al., 2007). The *STAT3* gene is located immediately downstream of the *STAT5A* gene (Hennighausen & Robinson, 2008; Teglund et al., 1998). STAT3 is a regulator of immune response genes, such as cytokines and inflammatory/immune mediators (Grivennikov & Karin, 2010; Lu et al., 2009). It is activated by the phosphorylation of its tyrosine 705 residue and dimerization of its reciprocal phosphotyrosine-SH2 domains (Yang et al., 2007). STAT3 binds the GAS sequence, TTCNNNGAA, in the promoters of induced genes (Yang et al., 2007). When deleted, it causes embryonic lethality, the only individual STAT to do so (Lu et al., 2009).

Activation of STAT3 is caused by many components of diabetes, which include reactive oxygen species, advanced glycation products, angiotensin II (primarily in mesangial cells), and high glucose (Lu et al., 2009). STAT3 is thought to play a critical role in acute kidney injury by mediating epithelial-mesenchymal transitions, apoptosis, and inflammation of the renal tubular epithelial cells (Matsui & Meldrum, 2012). STAT3 has been shown to be an important mediator of diabetic nephropathy (Lu et al., 2009). STAT3 is activated by IL-6, a proinflammatory cytokine that has also been linked to diabetic complications such as DN (Lu et al., 2009). Mice engineered to have only a quarter of normal STAT3 activity have significantly less mesangial expansion, glomerular cell proliferation, proteinuria, and macrophage infiltration in response to diabetes than mice with 75% of normal STAT3 activity (Matsui & Meldrum, 2012). The 25% STAT3 activity mice also showed reduced mRNA expression of monocyte chemotactic protein 1, nuclear factor κB, IL-6, intracellular adhesion molecule 1, type IV collagen, and transforming growth factor β1 when compared to the 75% STAT3 activity mice (Matsui & Meldrum, 2012).

Activation of phosphorylated STAT3 by IL-6 leads to an increase in unphosphorylated STAT3 (Jamieson et al., 2012; Yang et al., 2005; Yang et al., 2007). This was found specifically in kidney and spleen tissue (Narimatsu et al., 2001). Unphosphorylated STAT3 in turn can activate NFκB as was demonstrated in hTERT-HME1 cells (Fig. 4) (Grivennikov & Karin, 2010; Yang et al., 2007). Unphosphorylated STAT3 can displace IκB, a repressor of NFκB activity, and thus activate NFκB (Grivennikov & Karin, 2010; Jamieson et al., 2012; Yang et al., 2007). The unphosphorylated STAT3/NFκB transcription factor complex binds to the κB elements and induces gene expression (Yang et al., 2007). NFκB increases transcription of genes encoding cytokines, chemokines, inhibitors of apoptosis, enzymes that produce secondary inflammatory mediators, and adhesion molecules (Bonizzi & Karin, 2004; Navarro-Gonzalez et al., 2011). A positive feedback loop for inflammatory responses is seen (Yang et al., 2007). IL-1, an important mediator of inflammation response, activates NFκB, which induces expression of IL-6. IL-6 promotes phosphorylation of STAT3, which leads to an increase in unphosphorylated STAT3, which leads to a further increase in NFκB activity and gene activation (Fig. 4) (Yang et al., 2007).

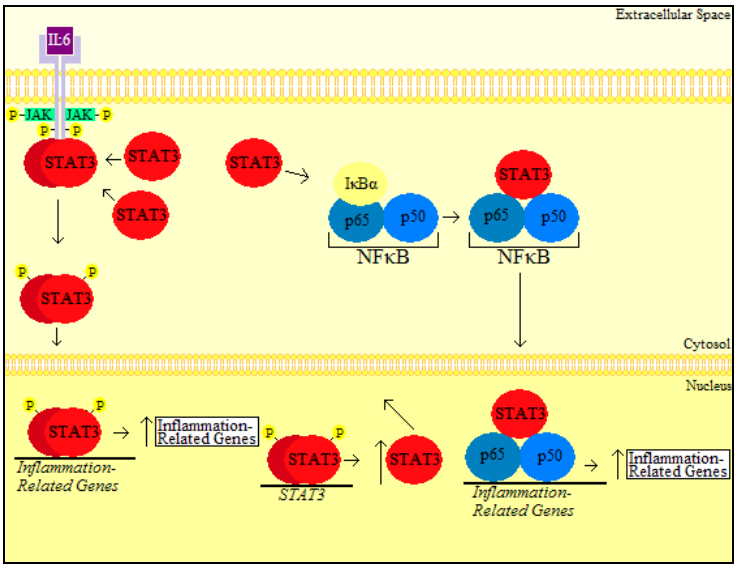

Figure 4. STAT3 pathway. Roles for phosphorylated and unphosphorylated forms of STAT3 in the regulation of inflammation-related gene expression are shown.

1.6 NFκB

The NFκB family has five members: RelA (p65), RelB, c-Rel, NF-κB1 (p105/p50), and NF-κB2 (p100/p52) (Baldwin, 1996; Bonizzi & Karin, 2004; Hayden & Ghosh, 2008). NF-κB1 and NF-κB2 are both synthesized as larger precursors, p105 and p100, respectively, that are post-translationally processed to form the respective DNA binding subunits, p50 and p52 (Baldwin, 1996; Bonizzi & Karin, 2004). This family has been characterized based on the Rel homology domain (Baldwin, 1996). This domain functions in specific DNA binding, homo- and heterodimerization, and interactions with IκB; it also contains the nuclear localization sequence (Baldwin, 1996; Bonizzi & Karin, 2004; Hayden & Ghosh, 2008). Only RelA, RelB, and c-Rel contain the transcriptional activation domain (Baldwin, 1996; Bonizzi & Karin, 2004; Hayden & Ghosh, 2008). Homodimers of p50 and p52 act as inhibitors; it is thought they do this because they do not contain a transcriptional activation domain (Bonizzi & Karin, 2004; Hayden & Ghosh, 2008).

Two tandem NFκB binding sites are required for the cytokine-mediated transcriptional activation of the *VCAM1* gene; both are necessary for the transcriptional response (Baldwin, 1996; Collins et al., 1995; Neish et al., 1995). The sites are located at positions -73 and -58 in the basal *VCAM1* promoter (Collins et al., 1995; Neish et al., 1995). It has been demonstrated that in TNFα activated endothelial cells, the *VCAM1* promoter is bound by the NF-κB heterodimer p50 (NF-κB1) and p65 (RelA) (Collins et al., 1995; Neish et al., 1995).

The p50/p65 heterodimer is considered to be the classic NFκB (Baldwin, 1996; Bonizzi & Karin, 2004). This dimer binds the sequence 5’ GGGRNNYYCC 3’ (Y is pyrimdine, R is purine) (Baldwin, 1996). Increased transcription of genes encoding cytokines, chemokines, inhibitors of apoptosis, enzymes that produce secondary inflammatory mediators and adhesion molecules are associated with classic NFκB (Bonizzi & Karin, 2004). The innate immune response uses these molecules to induce genes for the migration of phagocytic and inflammatory cells to the tissues where injury or infection has activated NF-κB.

IκB proteins are specific inhibitors of NFκB. There are six members in the IκB family: IκBα, IκBβ, IκBε, IκBγ, IκBξ, and Bcl-3 (Bonizzi & Karin, 2004; Hayden & Ghosh, 2008). The IκB proteins contain 6-7 ankyrin repeats; these are also found in the p100 and p105 proteins (Baldwin, 1996; Bonizzi & Karin, 2004; Hayden & Ghosh, 2008). IκB binds to the Rel homology domain of the NFκB dimer via these ankyrin repeats and blocks the nuclear localization sequence, retaining the dimer in the cytoplasm (Baldwin, 1996; Bonizzi & Karin, 2004). A single IκB protein interacts with a dimer of NF-κB (Baldwin, 1996).

Blocking of the nuclear localization signal for the p50/p65 heterodimer is complex (Hayden & Ghosh, 2008). IκBα only binds to the Rel homology domain of the p65 subunit, leaving the nuclear localization sequence of p50 and the nuclear export sequence of IκBα exposed (Hayden & Ghosh, 2008). This causes the constant shuttle of the p50/p65/IκBα complex to and from the nucleus to the cytoplasm. Once IκBα is degraded, the p50/p65 heterodimer becomes localized to the nucleus.

IκB proteins are degraded by the IκB kinase (IKK) complex (Hayden & Ghosh, 2008). IKK is activated by pathogen-associated molecular patterns and proinflammatory cytokines (Bonizzi & Karin, 2004). Usually the IKK complex is made up of catalytic subunits, IKKα and IKKβ, and a regulatory subunit, IKKγ (also known as NFκB essential modulator, NEMO) (Bonizzi & Karin, 2004). IKKα and IKKβ homo- and hetero-dimerize (Bonizzi & Karin, 2004). The activated IKK complex, in the classical NF-κB pathway, catalyzes phosphorylation, polyubiquitination, and finally degradation of the IκB protein by the 26S proteasome. When the NFκB dimers are released, they move into the nucleus, bind DNA, and activate transcription of target genes.

1.7 SKO Diabetic Nephropathy Study

Using the hypomorphic STAT5A and STAT5B double-knockout mouse line (SKO) originally described by Teglund et al. (Teglund et al., 1998), our lab investigated the effect of streptozotocin (STZ)-induced type 1 diabetes in kidneys of male SKO mice and their nontransgenic siblings (Fig. 5). Four groups of mice were studied: nondiabetic

nontransgenic mice (ND NT), diabetic nontransgenic mice (DB NT), nondiabetic STAT5A/B knockout mice (ND SKO), and diabetic STAT5A/B knockout mice (DB SKO). After 11 weeks of diabetes, substantial urinary albumin excretion and tubulointerstitial damage in the DB SKO mice was observed in comparison to the other three groups (Coschigano *et al*., unpublished data). Significant upregulation of inflammation-related gene expression in the kidneys of DB SKO mice in comparison to the other mouse groups was also seen, including the gene for vascular cellular adhesion molecule (VCAM)-1 (Coschigano *et al*., unpublished data).

Figure 5. Male nondiabetic, nontransgenic and STAT5A/B knockout mice.

VCAM-1 is 110 kDa in size and is a member of the immunoglobulin gene superfamily (Collins et al., 1995; Koga, Otsuki, Kubo, Hashimoto, & Kasayama, 1998; Luis-Rodriguez et al., 2012). Upregulation of VCAM-1 occurs in response to inflammatory cytokines (Navarro-Gonzalez et al., 2011). VCAM-1 has been suggested to have a role in diabetic nephropathy by binding monocytes and mediating their transmigration into the kidneys (Collins et al., 1995; Luster, Alon, & von Andrian, 2005; Navarro-Gonzalez et al., 2011). Accordingly, a significant increase in macrophage infiltration was observed in the kidneys of diabetic SKO mice in comparison to the other mouse groups (Coschigano *et al*., unpublished data).

NFκB is one of the major transcription factors for VCAM-1 (Collins et al., 1995; Neish et al., 1995). In keeping with the increased VCAM-1 expression previously observed, a significant increase in the DNA binding activity of NFκB in the DB SKO

mice in comparison to the other mouse groups was also observed (Coschigano et. al., unpublished data). Interferon regulatory factor 1 (IRF-1) works with NF-κB in cooperative DNA binding and transactivation of cytokine induction of VCAM-1 (Collins et al., 1995; Neish et al., 1995). It is necessary for the cell to fully respond to TNF-α stimulus (Neish et al., 1995). IRF-1 binds to the positively acting functional domain sequence GAAATAGAAA in the *VCAM1* promoter (Neish et al., 1995). Together, IRF-1 and NF-κB synergistically activate transcription of *VCAM1* (Neish et al., 1995).

1.8 IRF Family

IRF-1 belongs to the IRF family of proteins (Yu-Lee, 2001). The mammalian IRF family has nine members, IRF-1 through IRF-9 (Paun & Pitha, 2007; Savitsky, Tamura, Yanai, & Taniguchi, 2010; Yanai, Negishi, & Taniguchi, 2012). IRF proteins are transcription mediators of bacteria-, virus-, and interferon-induced signaling pathways. They play crucial roles in immune response, cell growth regulation, antiviral defense, and apoptosis (Paun & Pitha, 2007). Overlapping but distinct sets of target genes stimulated by active IRFs shape the appropriate immune response (Yanai et al., 2012).

Each of the IRF members have an N-terminal DNA-binding domain that is distinguished by a series of five well-conserved tryptophan-rich repeats (Paun & Pitha, 2007; Savitsky et al., 2010; Yanai et al., 2012). The domain is a helix-turn-helix structure that recognizes the DNA sequence interferon (IFN)-stimulated response element (ISRE), which is characterized by the consensus sequence 5′-$^{A}/_{G}$NGAAANNGAAA-3′ (Savitsky et al., 2010; Yanai et al., 2012).

The C-terminal region is not as conserved and allegedly mediates the interactions of a specific IRF with other family members, other transcription factors, or cofactors, which is how each IRF member has a specific function (Yanai et al., 2012). Nonetheless, two types of association modules have been found in the C-terminal region of the IRFs. In all IRFs except IRF-1 and IRF-2, there is a conserved IRF-associated domain I (IAD1); IAD2 is shared by IRF-1 and IRF-2. The protein-protein interactions dictated by

these domains may determine if the protein complex functions as a repressor or activator (Savitsky et al., 2010).

1.9 IRF-1

IRF-1 has distinct protein domains that mediate heterodimerization with IFN consensus sequence binding protein (ICSBP), nuclear translocation, DNA binding, and transcriptional activation (Kroger, Koster, Schroeder, Hauser, & Mueller, 2002). The DNA-binding domain is encoded by the N-terminal 125 amino acids and is conserved through the IRF family (Kroger et al., 2002). IRF-1 binds DNA either as a dimer or a monomer (Kroger et al., 2002). The consensus IRF-1 binding sequence motif is 5′-G(A)AAA$^{G}/_{C}{}^{T}/_{C}$GAAA$^{G}/_{C}{}^{T}/_{C}$-3′ (Kroger et al., 2002).

Between amino acids 185 and 256 of the IRF-1 protein are two activator regions that function in an additive manner (Kroger et al., 2002). A C-terminal region acts as a strong enhancer of these activator sequences, though it does not have any activator function. The N-terminal 60 amino acids act as a novel type of repression domain in IRF-1; it strongly inhibits the transcriptional activity of IRF-1 and is conserved in some but not all IRF family members (Kroger et al., 2002). This domain might exist to balance IRF-1 activity, which is regulated in various ways but mainly at the level of transcription (Kroger et al., 2002). IRF-8/ICSBP and IRF-2 act as functional antagonists of IRF-1. IRF-1 also cooperates with other transcription factors, such as NFκB. This interaction is important for the induction of several promoters.

IRF-1 protein is constitutively localized in the nucleus (Kroger et al., 2002). It has two nuclear localization sequences, ^{132}KSKTKRK and ^{120}RKERKSK. It is expressed at a low basal level in all examined cell types, except in early embryonic cells. IRF-1 mRNA levels accrue in response to some hormones, double-stranded RNA, interferon, retinoic acid, developmental cues, and cytokines (Kroger et al., 2002; Yu-Lee, 2001). The mRNA levels of IRF-1 are probably reflected in the protein levels since the proteins only have a half-life of thirty minutes (Kroger et al., 2002).

In the proximal promoter region of the *IRF1* gene, a number of DNA elements are targets of specific signaling proteins (Yu-Lee, 2001). These include IFNγ activated sequences (GAS) at -110 and -120 bp and binding sites for NFκB at -35 and -45 bp, Sp1 at -200 bp and Yi at -180 bp. GAS and NFκB bindings sites are the key promoter elements for *IRF1* gene transcription (Kroger et al., 2002). These sites bind STAT1 and NFκB to mediate transcription.

The *IRF1* gene promoter is an NFκB target promoter in which NFκB is inhibited by STAT5B (Yu-Lee, 2001). *IRF1* gene transcription is activated by PRL- or IFNγ-inducible STAT1 and tumor necrosis factor α (TNFα)-inducible NFκB (Pine, 1997; Yu-Lee, 2001). TNFα and IFNγ synergistically induce *IRF1* expression (Pine, 1997). In opposition it has been shown that PRL-induced STAT5B inhibits transcription of the *IRF1* gene by NFκB and STAT1 (Fig. 6) (Luo & Yu-Lee, 2000; Yu-Lee, 2001). The possible mechanism for this is that STAT5B sequesters a limiting cofactor (p300/CBP) at the target promoter (Luo & Yu-Lee, 2000; Yu-Lee, 2001).

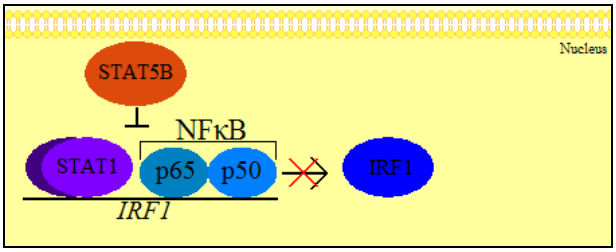

Figure 6. STAT5B repressor pathway. NFκB-induced transcription of the IRF1 gene is repressed by STAT5B.

CHAPTER 2: HYPOTHESIS AND SPECIFIC AIMS

Diabetic nephropathy is currently the leading cause of end-stage renal disease and renal failure in humans (Luis-Rodriguez et al., 2012; Navarro-Gonzalez et al., 2011). It is known that an activated innate immunity, with a chronic low-grade inflammation, contributes to the pathogenesis of diabetic nephropathy (Luis-Rodriguez et al., 2012). What is not well known are the pathways that lead to this disease (Luis-Rodriguez et al., 2012). Defining these pathways is important as they have the possibility to show new drug targets (Luis-Rodriguez et al., 2012; Navarro-Gonzalez et al., 2011).

The long-term goal of this research is to find possible drug targets in order to treat or prevent diabetic nephropathy. The overall objective of this work, which was the next step toward attainment of the long-term goal, was to explain the effect of the absence of STAT5A/B in diabetic kidneys, which leads to a significant increase in inflammation-related gene expression and macrophage infiltration (Coschigano *et al*., unpublished data). The central hypothesis is that the combination of the loss of STAT5 repression and increase of STAT3 activity escalates inflammation-related gene expression in the kidneys of diabetic STAT5A/B knockout mice.

It has been shown that STAT5B inhibits the NFκB and STAT1 transcriptional activation of IRF-1 in COS-1 cells, likely through competitive binding of common transcription factors (Luo & Yu-Lee, 2000); thus, STAT5 absence would lead to an increase in IRF-1 RNA expression, and likely other inflammation-related genes. It has also been shown that STAT3 levels increase with the loss of STAT5A/B (Cui et al., 2007). Both phosphorylated and unphosphorylated STAT3 have been shown to have roles in the activation of inflammation-related gene expression (Grivennikov & Karin, 2010; Lu et al., 2009; Yang et al., 2007).

The central hypothesis was tested with the following two specific aims:

1. **To determine the expression levels of the *IRF1* gene (RNA and protein) in diabetic SKO kidneys.**

   Based on previous data, the working hypothesis was that loss of STAT5 repression of NFκB and STAT1 transcriptional activity would result in a significant increase of *IRF1* RNA, which in turn could lead to a significant increase in IRF-1 protein since the level of RNA appeared to correspond with protein levels (Kroger et al., 2002). Since IRF-1 and NFκB are the two major transcription factors for VCAM-1 (Collins et al., 1995; Neish et al., 1995), a significant increase in IRF-1 protein could lead to the significant increase in *VCAM1* RNA and protein levels that were observed in kidneys of diabetic SKO mice, which in turn could lead to the significant increase in macrophage infiltration previously observed (Coschigano *et al*., unpublished data).

2. **To determine the levels of phosphorylated and unphosphorylated STAT3 protein and RNA levels of STAT3-regulated genes in diabetic SKO mice.**

   Based on previous data, the working hypothesis was that there would be a significant increase in levels of STAT3 protein as a result of the absence of STAT5 (Matsui & Meldrum, 2012). Phosphorylated STAT3 is known to increase the amount of unphosphorylated STAT3, which in turn activates NFκB (Grivennikov & Karin, 2010; Yang et al., 2007). Both phosphorylated STAT3 and activated NFκB lead to activation of inflammation-related gene expression (Grivennikov & Karin, 2010; Lu et al., 2009; Yang et al., 2007). Thus, increases of phosphorylated and unphosphorylated STAT3 resulting from the absence of STAT5 could also cause the increased inflammation-related gene expression observed in diabetic SKO kidneys.

CHAPTER 3: MATERIALS AND METHODS

3.1 Mice

The STAT5A and STAT5B knockout mouse line used in this study originated from the lab of Dr. James Ihle. It was genetically engineered to have a deletion in the first coding exon of the STAT5A and STAT5B genes which truncates the N-terminus of the proteins and prevents tetramer formation (Hennighausen & Robinson, 2008; Teglund et al., 1998). Truncated protein is detected at 1% or less of the normal protein levels (Teglund et al., 1998). This makes them hypomorphic for STAT5A and STAT5B (Hennighausen & Robinson, 2008; Teglund et al., 1998). A colony was established and maintained at Ohio University through the breeding of heterozygote males and females on a mixed genetic background of C57Bl/6 and 129/SvE (Teglund et al., 1998). Mice were housed in micro-isolator caging with a 14h light/10h dark cycle. They were given reverse osmosis water and standard rodent chow (Prolab RMH 3000, PMI Nutrition International, Inc., Brentwood, NJ) *ad libitum*. Protocols were approved by the Ohio University Institutional Animal Care and Use Committee and followed federal, state, and local guidelines.

Progeny mice were genotyped by polymerase chain reaction (PCR) followed by electrophoresis and visualization of the resulting products. Genomic DNA was extracted from ~2 mm tail clips using a standard alkaline lysis method. In short, 100 µL of NaOH solution (25 mM NaOH, 0.2 mM EDTA, pH 8) was added to the microcentrifuge tube containing the tail clip and placed on a heat block for 30 minutes at 100°C. The tube was then centrifuged at 18,400 ×g for 30 seconds. 100 µL of Tris solution (40 mM Tris-HCl, pH ~5) was added to the tube and the tube vortexed for approximately 5 seconds. 2 µL of this DNA was used for genotyping. Extracted DNA was stored at 4°C.

The master mix for genotyping the STAT5A deletion consisted of 9.925 µL nuclease-free water, 1.5 µL 10× ThermoPol Reaction Buffer (New England Biolabs® (NEB), Ipswich, MA, cat # B90045), 0.3 µL Deoxynucleotide Solution Mix (NEB, cat # N0447S, 10 mM of each dNTP), 0.45 µL of 20 µM F9(3KC) primer, 0.45 µL of 20 µM

R1(4KC) primer, 0.225 µL of 20 µM TKp primer, and 0.15 µL Taq Polymerase (NEB, cat # M0267L ; 5 units / µL) for a total of 13 µL per reaction. 2 µL of genomic DNA or nuclease-free water was then added to each tube. Primer sequences are listed in Table 1.

Table 1

Genotyping Primers

Primer Pair	**Sequence (5′→3′)**	**T_M (°C)**	**Amplified Gene**	**Product Size (bp)**
F9(3KC)	GTCTGGGGATAGCTCCATC	54.4	STAT5A	257
R1(4KC)	CGCCATGGCTGTTTACCTG	56.7		
F9(3KC)	GTCTGGGGATAGCTCCATC	54.4	STAT5A KO	~150
TKp	GCAAAACCACACTGCTCGAC	57.1		
F11	TCAAACACACCTCAATTAGTCC	52.7	STAT5B	400
R8	GGAGATCTGCTGGCTGAAAG	55.6		
TKp	GCAAAACCACACTGCTCGAC	57.1	STAT5B KO	~150
R8	GGAGATCTGCTGGCTGAAAG	55.6		

The master mix for genotyping the STAT5B deletion consisted of 9.925 µL nuclease-free water, 1.5 µL 10× ThermoPol Reaction Buffer (NEB), 0.3 µL Deoxynucleotide Solution Mix (NEB), 0.45 µL of 20 µM F11 primer, 0.45 µL of 20 µM R8 primer, 0.225 µL of 20 µM TKp primer, and 0.15 µL Taq Polymerase (NEB) for a total of 13 µL per reaction. 2 µL of genomic DNA or nuclease-free water was then added to each tube.

PCR was performed in an iCycler thermal cycler (Bio-Rad, Hercules, CA) using the following protocol: 94°C for 2 minutes; 30 cycles of 94°C for 15 seconds, 60°C for 30 seconds, 72°C for 30 seconds; and then a hold at 16°C until the reaction was removed from machine.

When cycling was complete, PCR reactions were mixed with 2 µL of xylene cyanol in 50% glycerol and electrophoresed for 25 minutes at 100 volts through a 2% agarose gel with 20 µg ethidium bromide/100 mL gel added for visualization. The gel

was imaged on a ChemiDoc™ XRS™ digital imager (Bio-Rad) using Image Studio version 2.0.1 software.

Diabetes was induced in homozygous double knockout (STAT5A$^{-/-}$ and STAT5B$^{-/-}$ or SKO) or nontransgenic (NT) male sibling mice using the Mouse Models of Diabetic Complications Consortium low-dose streptozotocin induction protocol (mouse) written by Frank Brosius in 2003 (www.diacomp.org/shared/showFile.aspx?doctypeid=3&docid=19). Briefly, an intraperitoneal injection of streptozotocin (50-55 mg/kg body weight; 7.5 mg/ml in 50 mM Na-citrate, pH 5.0) or Na-citrate vehicle was administered to ~8 week old mice once a day for five consecutive days, creating four groups of mice: nondiabetic nontransgenic (ND NT), diabetic nontransgenic (DB NT), nondiabetic SKO (ND SKO), and diabetic SKO (DB SKO), ten mice per group. The date of the first of two consecutive weekly glucose readings of greater than 300 mg/dl, measured after a 4-6 hr fast using a Lifescan Genuine One Touch glucometer (Johnson and Johnson, New Brunswick, New Jersey) and a drop of blood from the tip of the tail was used to define the start of diabetes. Diabetic mice were only used for this study if they had ketone levels less than 5 mg/dl, urinary glucose levels greater than 1000 mg/dl, and no more than ~20% body weight loss. Diabetic mice and age matched nondiabetic controls were euthanized after ~11 weeks of diabetes. Kidneys were immediately harvested, frozen in liquid nitrogen and then stored at -80°C.

3.2 cDNA Synthesis

Total RNA was previously isolated from frozen kidney samples of each mouse in the four mouse groups. In brief, ~20 mg of frozen kidney was homogenized in Stat-60 (Tel-Test, Inc., Friendswood, TX, cat # CS-111) according to the manufacturer's instructions. After homogenization, chloroform (EMD Biosciences, Inc., La Jolla, CA, cat # 516726) was added, shaken vigorously and incubated at room temperature for three minutes. The tube was then centrifuged for 15 minutes at 4°C at 18,400 ×g. The aqueous layer was transferred to a RNase-free microcentrifuge tube containing 250 µL isopropanol. This was mixed by inversion several times and incubated at room

temperature for 10 minutes. The tube was then centrifuged for 10 minutes at 4°C at 18,400 ×g. Supernatant was discarded and 1 mL of 70% ethanol was added. The tube was vortexed and centrifuged for 5 minutes at 4°C at 7500 ×g. Supernatant was discarded again and the pellet was air dried for 10 minutes without drying completely. The pellet was resuspended in 30 µL nuclease-free H_2O. The "dirty" RNA (potentially contaminated with genomic DNA) was quantitated by diluting 2 µL of RNA in 2 µL nuclease-free H_2O and placing 1 µL of solution on the pedestal of a Nanodrop 2000c spectrophotometer (ThermoScientific, Wilmington, DE). A_{260} and A_{280} readings were used to determine concentration (µg/µL) and assess purity (A_{260}:A_{280}). RNA was stored at -80°C.

Genomic DNA was removed from the RNA samples by DNase I digestion following the RNeasy® Micro Kit instructions (Qiagen, Valencia, CA, cat # 74004). For each sample, several micrograms of "dirty" RNA was brought up to 87.5 µL with RNase-free water and 10 µl Buffer RDD and 2.5 µL of DNase stock solution were added. It was then incubated for 10 minutes at room temperature. This was followed by RNA clean-up according to the manufacturer's instructions. Purity and concentration of the DNase-treated RNA samples was determined by diluting the RNA with an equal volume of nuclease-free water and measuring absorbance at 260 and 280 nm.

cDNA was made from DNase-treated RNA using the iScript cDNA synthesis kit (Bio-Rad, cat # 170-8891). A reaction mix consisted of 5 µL of nuclease-free water, 4 µL of 5× iScript Reaction Mix, and 1 µL of iScript reverse transcriptase for a total of 10 µL. A calculated volume for 1 µg of DNase-treated RNA plus nuclease-free water in a total volume of 10 µL was added to each reaction mix for a final volume of 20 µl. The tubes were then placed in the iCycler thermal cycler (Bio-Rad) for synthesis using a protocol of 25°C for 5 minutes, 42°C for 30 minutes, 85°C for 5 minutes, and finally 4°C until removed from machine. The cDNA was then stored at -80°C.

3.3 Protein Lysates

Protein lysates were extracted from frozen kidney samples using reagents from the TransAM™ NFκB Chemi kit (Active Motif, cat # 40097), except for addition of

Phosphatase Inhibitor Cocktail (100×, Active Motif, cat # 100567). A protein extraction mix containing 97.5 µL of Lysis Buffer AM2, 1 µL each of 100× Protease Inhibitor Cocktail and 100× Phosphatase Inhibitor Cocktail, and 0.5 of 1 M DTT was added to an Eppendorf Lock-tite microcentrifuge tube, along with approximately 20 mg of frozen kidney sample and 60 mg of RNase- and DNase-free 0.5 mm diameter zirconium oxide beads (NEXT>>>ADVANCE, Averill Park, NY, cat # ZrOB05). The tube was then processed in the Bullet Blender (NEXT>>>ADVANCE) for 5 minutes at a setting of 10 at 4°C. The samples were checked after homogenization and, if not fully homogenized, the homogenization was repeated for an additional 5 minutes. After complete homogenization, the sample was centrifuged at 18,400 ×g for 5 minutes at 4°C and then the supernatant was transferred to PCR tubes for storage at -80°C.

Protein was quantified using a Micro BCA™ Protein Assay kit (Thermo Scientific, Rockford, IL, cat # 23235) with bovine serum albumin (BSA) as the standardizing protein. The standard curve was prepared using the concentrations of 2000 µg/mL, 1500 µg/mL, 1000 µg/mL, 750 µg/mL, 500 µg/mL, 250 µg/mL, and 125 µg/mL of BSA. 25 µL of each diluted standard, or 1.25 µL of each kidney sample plus 23.75 µL of nuclease-free water, was assayed, in duplicate, in a 96-well microplate. 200 µL of the working reagent, consisting of 50 parts A reagent, 40 parts B reagent, and 1 part C reagent, were added to each well. The plate was covered, mixed on a plate shaker for 30 seconds, and then incubated at 37°C for 30 minutes. Absorbance at 562 nm was read using a SynergyHT plate reader (BioTek®) and Gen5™ Program version 1.10. Protein concentration was determined by comparison to the standard curve after subtraction of the no protein (blank) control. One sample, Mouse 179, was excluded from all the protein assays due to not having enough kidney to create a protein lysate.

3.4 *IRF1* Primer Design

Primers for the *IRF1* gene were designed using the Primer-BLAST program (Ye et al., 2012). Primer-BLAST uses the program Primer3 version 4.0.0 and BLAST to design primers (Rozen & Skaletsky, 2000). The primers were synthesized by Integrated

DNA Technologies (IDT, Coralville, IA). The positive strand primer was 25 nucleotides long, 5′-GACCTTATGAAGCTCTTTGAACGT-3′, and spanned the junction of exon 9 and 10. The negative strand primer, 5′-AACGGGTCAGAGACCCAAAC-3′, was 20 nucleotides long and located within exon 11. The amplified product length was 301 bp.

Primer efficiency tests were performed to assess how well primers for real time RT-PCR analysis amplify product; melt curve analyses checked the specificity of the primers, i.e. amplification of a single product. Primer efficiency was determined using the iQ™ SYBR® Green Supermix (Bio-Rad, cat # 170-8882). Previously created cDNA from several kidney samples were pooled and then serially diluted in 3-fold increments (1/1, 1/3, 1/9, 1/27, 1/81). Each PCR reaction contained 4 µL of nuclease-free water, 12.5 µL of iQ™ SYBR® Green Supermix, and 1 µL of the appropriate cDNA dilution for a total of 17.5 µL per well. The *IRF1* primer pair mix for each well contained 7.125 µL of nuclease-free water, 0.375 µL of 20 µM positive strand primer, and 0.375 µL of 20 µM negative strand primer, for a total of 7.5 µL per well. The total reaction volume (cDNA mix plus primer mix) per well was 25 µL.

Amplification was monitored in a MyIQ™ Single Color Real Time PCR Detection System (Bio-Rad) using the software Bio-Rad iQ5 version 2.0. Real-time RT-PCR was performed using the protocol of 95°C for 3 minutes; 40 cycles of 95°C for 15 seconds, 55°C for 30 seconds, 72°C for 30 seconds; followed by melt curve analysis: 95°C for 1 minute; 55°C for 1 minute; and 55°C to 95°C, increasing 0.5°C every 10 sec for 80 cycles. Fluorescence was measured during the 72°C extension step.

After real time analysis, amplified products of the *IRF1* primer pair were mixed with loading dye containing xylene cyanol plus 50% glycerol and electrophoresed through a 2% agarose gel with 20 µg ethidium bromide/100 mL gel for 25 minutes at 100 volts. The gel was imaged on the ChemiDoc™ XRS™ (Bio-Rad) using Image Lab version 2.0.1 software.

Further validation of the primer efficiency results were performed with an alignment of *IRF2* sequence with the forward primer and then with the reverse compliment of the reverse primer. The alignment was run in the program MEGA version 5.10 with the alignment tool ClustalW with the default settings.

3.5 Real Time RT-PCR

Relative amounts of *IRF1* RNA levels were determined using real time RT-PCR. Measurement of the housekeeping genes *GADPH* and *γ-actin* was used to normalize the data, controlling for variations in the amount of input RNA and efficiency of cDNA synthesis between samples. These were previously found to be the most stably expressed genes from a total of six housekeeping genes tested and have been used for all real-time RT-PCR experiments involving kidney RNA in the Coschigano lab. A negative control reaction containing no cDNA was included to determine if there was any DNA contamination of the reactions. Information about primer sequences and products are included in Table 2.

Table 2

Real Time RT-PCR Primers

Primer Pair	**Sequence (5′→3′)**	**TM (°C)**	**Amplified Gene**	**Product Size (bp)**
GAPDH (+)	TGTGTCCGTCGTGGATCTGA	58.1	GAPDH	77
GAPDH (-)	CCTGCTTCACCACCTTCTTGA	57.2		
γ-Actin (+)	ACCAACAGCAGACTTCCAGGAT	58.5	γ-Actin	76
γ-Actin (-)	AGACTGGCAAGAAGGAGTGGTAA	57.8		
IRF-1 var 1,2,3 (+)	GACCTTATGAAGCTCTTTGAACAGT	55.1	IRF-1, var 1 and 2	301
IRF-1 var 1,2 (-)	AACGGGTCAGAGACCCAAAC	57.3		

A cDNA mix was made consisting of, per reaction: 4.5 µL of nuclease-free water, 12.5 µL of iQ™ SYBR® Green Supermix, and 0.5 µL of cDNA for a total volume of 17.5 µL for each well. The primer pair mix for each well contained 7.125 µL of nuclease-free water, 0.375 µL of 20 µM positive strand primer, and 0.375 µL of 20 µM negative strand primer, for a total of 7.5 µL per well. The total real time reaction volume (cDNA mix plus primer mix) per well was 25 µL. Amplification and fluorescence monitoring was performed as described for the primer efficiency test. Each kidney sample was run in

duplicate on a single plate and then completely replicated on a second plate for each primer pair.

For each IRF1 plate, cycle threshold (Ct) values were converted to linear quantity values according to the delta Ct method (Andersen, Jensen, & Orntoft, 2004). IRF1 quantity values were then normalized for each sample by dividing each by the geometric mean of the corresponding quantity values for the two most stable housekeeping genes, *γ-Actin* and *GAPDH*, previously selected from a larger group of housekeeping genes using a model-based variance estimation approach (Andersen et al., 2004). Normalized values were finally compared between groups, relative to the ND NT group.

After real time analysis, amplified products from the first two mice of each group on the first IRF1 plate were mixed with loading dye containing xylene cyanol plus 50% glycerol and electrophoresed through a 2% agarose gel with 20 μg ethidium bromide/100 mL gel for 25 minutes at 100 volts. The gel was imaged on the ChemiDoc™ XRS™ digital imager (Bio-Rad) using Image Lab version 2.0.1 software.

3.6 IRF-1 Western Blot Analysis

Relative IRF-1 protein levels were assessed by western blot analysis. 30 μg of kidney protein lysate, brought to a volume of 7.5 μL with nuclease-free water, was mixed with 7.5 μL of Laemmli Sample Buffer (Bio-Rad, cat # 161-0737) with 5% 2-mercaptoethanol (OmniPur, cat # 6010), heated at 70°C for 10 min and then electrophoresed through a 7.5% acrylamide Mini-Protean® TGX™ gradient gel (Bio-Rad, cat # 456-1026) in the Mini-Protean® 3 (Bio-Rad) at 200 volts for ~29 min in 25 mM Tris, 192 mM glycine, 0.1% (w/v) SDS, pH 8.3 running buffer made from a 10× TGS stock (Bio-Rad, cat # 161-0772).

In the Mini Trans-Blot® Electrophoretic Transfer Cell (Bio-Rad), separated proteins were then transferred from the gel to a nitrocellulose membrane (Li-COR, cat # 926-31092) in chilled transfer buffer (25 mM Tris, 192 mM glycine, pH 8.3, 20% methanol) at 100 volts for 1 hour. Transfer buffer was made from a 10× TG stock (Bio-Rad, cat # 161-0771) and methanol (J.T. Baker, Phillipsburg, NJ, cat # 9098-13). After

transfer, the nitrocellulose membrane was air-dried, blocked for 1 hour at room temp with gentle rocking in Odyssey® Blocking Buffer (Li-COR, cat # 927-40000) and then incubated overnight at 4°C with gentle rocking with a rabbit monoclonal antibody to IRF-1 (Cell Signaling Technology®, cat # 8478P) diluted 1:1000 in Odyssey® Blocking Buffer in a total volume of 15 mL. The next day the membrane was washed three times for 5 to 10 minutes with wash buffer (1× PBS, 0.2% Tween 20). Wash buffer was made from a 10× PBS stock (AMRESCO®, Solon, OH, cat # J373-4L) and 10% Tween 20 (Bio-RAD, cat # 161-0781). This was followed by incubating for an hour with the 800CW IRDye labeled goat anti-rabbit (Li-COR, cat # 926-32211) secondary antibody diluted 1:15,000 in Odyssey® Blocking Buffer for a total volume of 15 mL at room temp with gentle rocking. Membrane was again washed three times for 5 to 10 minutes with wash buffer and rinsed twice in 1× PBS. Rinse buffer was made from a 10× PBS stock (AMRESCO®, cat # J373-4L). The membrane was then imaged on the Odyssey Infrared Imaging System (Li-COR) using the Odyssey Infrared Imaging System Application software version 3.0.30.

The constitutively expressed protein β-actin was used as a normalization control. After imaging for IRF1, the membrane was blocked for thirty minutes at room temp with Odyssey® Blocking Buffer and then incubated overnight at 4°C with goat polyclonal to β-actin (Abcam, cat # ab8229) diluted 1:1000 in Odyssey® Blocking Buffer. Membrane was washed as described earlier, followed by an hour incubation at room temp with a 680RD IRDye labeled donkey anti-goat (Li-COR, cat # 926-68074) secondary antibody diluted 1:15,000 in Odyssey® Blocking Buffer. Membrane was again washed as before and rinsed twice in 1× PBS. The membrane was imaged again on the Odyssey infrared imaging system.

Image Studio Version 3.1 (Li-COR) was used to quantify band signal. Specific bands were outlined by a user-defined rectangle, using the same sized box for each band. Background noise was determined by the program by defining the average pixel intensity in the top and bottom background segment of each rectangle. The program determined the signal of each band by adding the individual pixel intensity values contained within a user-defined rectangle surrounding each band and subtracting the product of the total

number of pixels enclosed by the rectangle and the average intensity values of the background pixels. Data was normalized by dividing the signal of IRF-1 by the signal of β-actin. The western blot analysis was repeated twice per mouse kidney lysate.

3.7 STAT3 Western

A specific antibody exclusively recognizing unphosphorylated STAT3 protein does not exist; therefore, relative levels of total STAT3 protein were determined. This included both phosphorylated and unphosphorylated STAT3.

Relative levels of phosphorylated and total STAT3 protein levels were determined by performing western blot analysis as described above. Phosphorylated STAT3 was assayed first and the membrane imaged. After imaging, the membrane was blocked with Odyssey® Blocking Buffer for 30 minutes and then total STAT3 was analyzed. The primary antibody for phosphorylated STAT3 was a rabbit monoclonal antibody against STAT3 phosphorylated at tyrosine 705 (Cell Signaling Technology®, cat # 9145P) diluted 1:2000 in Odyssey® Blocking Buffer. The secondary antibody was an 800CW IRDye labeled goat anti-rabbit diluted 1:15,000 in Odyssey® Blocking Buffer. Total STAT3 protein was detected with a mouse monoclonal antibody (Cell Signaling Technology®, cat # 9139S) diluted 1:1000 in Odyssey® Blocking Buffer; the secondary antibody was a 680LT IRDye labeled goat anti-mouse (Li-COR, cat # 827-11080) diluted 1:20,000 in Odyssey® Blocking Buffer.

Image Studio Version 3.1 (Li-COR) was used to quantify band signal. Background and signal were quantified as described above. Since phosphorylated STAT3, total STAT3, IRF-1, and β-actin for each protein sample were all analyzed on the same membranes, the β-actin signal determined earlier from that gel was used to normalize the STAT3 results as well. Data was normalized by dividing the signal for phosphorylated STAT3 and total STAT3 by the signal for β-actin.

3.8 STAT3 Milliplex Assays

Phosphorylated STAT3 protein levels were determined with MILLIPLEX™MAP 5-plex STAT Phosphoprotein Magnetic Bead Kit #48-610MAG (EMD Millipore, Billerica, MA) following the manufacturer's instructions. In short, after the samples were prepared and all the reagents were at room temperature (RT), the plate was wetted with 50 µL Assay Buffer, sealed and left on a plate shaker (600-800 rpm) for 10 minutes. The 1× bead mix was prepared by adding 150 µL of each of the 20× magnetic bead mixes in the kit, as well as MILLIPLEX™MAP β-Tubulin Magnetic Bead MAPmate® #46-713MAG (EMD Millipore) for normalization purposes, to a mixing bottle and then bringing the final volume up to 3 mL with Assay Buffer. The Assay Buffer was decanted from the plate and 25 µL of vortexed 1× bead mix was added to each well. Then, 25 µL of protein (20 µg lysate in Assay Buffer) or controls were added to appropriate wells. A titration of the positive control lysate was included to create a curve to determine if the sample signals fell within the linear part of the curve. The plate was sealed, protected from light, and incubated overnight at 4°C on a plate shaker (600-800 rpm).

After 16-20 hours, the plate was placed on a magnetic separation block for 60 seconds (this is done for each decanting step), and the samples/controls were decanted. The plate was hand washed by adding 100 µL of Assay Buffer to each well, mixing on a plate shaker for 30 seconds, placing the plate on the magnetic separation block for 60 seconds, and then decanting the Assay Buffer. The wash step was performed twice. 1× Detection Antibody was prepared by adding 150 µL of each of the 20× Detection Antibody stocks to a mixing bottle and then bringing the final volume up to 3 mL with Assay Buffer. 25 µL of 1× Detection Antibody was added to each well, sealed, and incubated for an hour at RT on the plate shaker. The antibody was then decanted. A volume of 25 µL of Streptavidin-Phycoerythrin (SAPE) was added to each well and incubated for 15 minutes at RT on the plate shaker (SAPE was made by adding 120 µL of SAPE stock to 2.88 mL of Assay Buffer). Then 25 µL of Amplification Buffer was added to each well and incubated for 15 minutes at RT on the plate shaker. The SAPE/Amplification Buffer were decanted and 150 µL of Assay Buffer was added and

mixed on a shaker at RT for 5 minutes. The plate was then read on a Milliplex Analyzer/Luminex LX100/LX200 (EMD Millipore) using the Lumniex xPonent software version 3.1. STAT3 signals were normalized by division by the β-Tubulin signal.

Total STAT3 protein levels were determined with a MILLIPLEX™MAP Total STAT3 MAPmate® kit #48-625MAG (EMD Millipore) following the manufacturer's instructions (as described above). 5 µg of protein plus Assay Buffer for a total volume of 25 µL per well was used. Again, a titration of the positive control lysate was performed to create a curve to see if the sample signals fell within the linear part of the curve and also MILLIPLEX™MAP β-Tubulin Magnetic Bead MAPmate® #46-713MAG (EMD Millipore) was included for normalization purposes.

As seen in *Yue et al.*, the total STAT3 protein was compared to the phosphorylated STAT3 to approximate unphosphorylated STAT3 (Yue, Li, Desnoyer, & Karnik, 2010). To approximate the signal for unphosphorylated STAT3, the ratio of phosphorylated STAT3 signal to total STAT3 signal was subtracted from one. This was done for each duplicate per mouse. Duplicates were matched up accordingly, such as #41 phosphorylated STAT3 duplicate 1 with #41 total STAT3 duplicate 1.

3.9 Statistical Analyses

Statistical analysis was performed under the guidance of Dr. Masato Nakazawa, the HCOM Biostatistician, using the software R i383 version 3.0.0 and RStudio version 0.97.449, along with programming code written by Dr. Nakazawa. Intra-class correlation (ICC) was performed to determine consistency between duplicates, and replicates when applicable; a value greater than 0.70 was considered to be consistent. Outliers were detected by computing the MAD score for each duplicate per mouse per assay and then taking the median of those MAD calculations for each molecule. Assays with an ICC score less than 0.70 were excluded from the calculation. If the final MAD score was over 2.81 that mouse was considered to be an outlier (Fig. 7).

Two-way Analysis of Variance (ANOVA) was performed for each data set with between-subject factors of Diabetes (DB vs. ND); and Genotypes (SKO vs. NT); a p

value less than 0.05 was considered to be significant. Fisher's Least Significant Difference (FLSD) test was run to test pair-wise comparisons without any alpha adjustments; a p value less than 0.05 was considered to be significant. Likelihood test was performed to determine if adding a duplicate random factor improved the model; if the p value was less than 0.05, then the ANOVA and FLSD were repeated adding that factor. Statistical analyses were performed for all datasets with and without the calculated outliers. This was to determine if the outliers had a significant influence on the data sets.

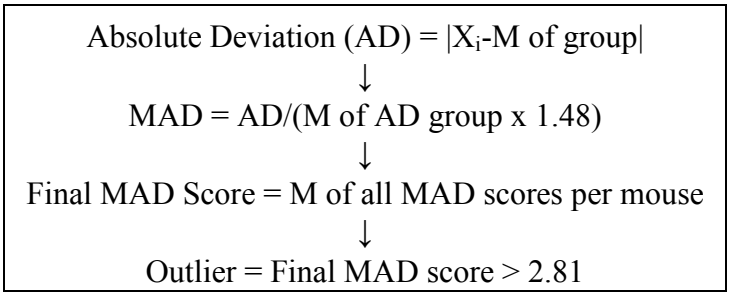

Figure 7. Flow chart for MAD calculations

CHAPTER 4: RESULTS

4.1 Evaluation of IRF1 Real Time RT-PCR Primer Efficiency

Primer efficiency was assessed to determine the effectiveness of the newly designed IRF1 primers. There were three *IRF1* variants found when searching the nucleotide database of NCBI (http://www.ncbi.nlm.nih.gov/nuccore), variant 1 (NM_008390.2), variant 2 (NM_001159396.1), and variant 3 (NM_001159393.1). According to the NCBI website (http://www.ncbi.nl m.nih.gov/gene/?term =NM_001159396.1), *IRF1* variants 1 and 2 encode an identical protein product (NP_001152865.1). *IRF1* variant 3 encodes a different protein product (NP_001152865.1). An alignment of protein sequences demonstrated that the two IRF-1 proteins differ only at the C-terminal end (Fig. 8). No publications were found which described in more detail the differences between these two proteins.

```
NP_001152868.1 - MPITRMRMRPWLEMQINSNQIPGLIWINKEEMIFQIPWKHAAKHGWDINKDACLFRSWAIHTGR
NP_001152865.1 - MPITRMRMRPWLEMQINSNQIPGLIWINKEEMIFQIPWKHAAKHGWDINKDACLFRSWAIHTGR

NP_001152868.1 - YKAGEKEPDPKTWKANFRCAMNSLPDIEEVKDQSRNKGSSAVRVYRMLPPLTRNQRKERKSKSS
NP_001152865.1 - YKAGEKEPDPKTWKANFRCAMNSLPDIEEVKDQSRNKGSSAVRVYRMLPPLTRNQRKERKSKSS

NP_001152868.1 - RDTKSKTKRKLCGDVSPDTFSDGLSSSTLPDDHSSYTTQGYLGQDLDMERDITPALSPCVVSSS
NP_001152865.1 - RDTKSKTKRKLCGDVSPDTFSDGLSSSTLPDDHSSYTTQGYLGQDLDMERDITPALSPCVVSSS

NP_001152868.1 - LSEWHMQMDIIPDSTTDLYNLQVSPMPSTSEAATDEDEEGKIAEDLMKLFEQSEWQPTHIDGKG
NP_001152865.1 - LSEWHMQMDIIPDSTTDLYNLQVSPMPSTSEAATDEDEEGKIAEDLMKLFEQSEWQPTHIDGKG

NP_001152868.1 - YLLNEPGTQLSSVYGDFSCKEEPEIDSPRGDIGIGIQHVFTEMKNMDSIMWMDSLLGNSVRLPP
NP_001152865.1 - YLLNEPGTQLSSVYGDFSCKEEPEIDSPRGNLLMGVFCWLSAWASAEH----------------

NP_001152868.1 - SIQAIPCAP
NP_001152865.1 - ---------
```

Figure 8. Alignment of the IRF-1 protein isoforms.

The first set of primers selected using Primer-BLAST utilized hybridization of a positive strand forward primer (to a sequence in common to all three *IRF1* variants (IRF-1 var 1,2,3 (+)) and hybridization of a negative strand reverse primer to a sequence in common only to variants 1 and 2 (IRF-1 var 1,2 (-)). The primers were predicted to

amplify a single common product 301 base pairs in size and thus assess the amount of variant 1 and 2 mRNAs combined (Fig. 9). With only 65% sequence identity between the negative strand IRF-1 var 1,2 (-) primer and variant 3 (Fig. 10), amplification of variant 3 was not expected under the reaction conditions used and, if occurring, would amplify a fragment 383 base pairs in size. A second pair of primers designed for *IRF1* variant 3 failed three separate efficiency tests with an efficiency of less than 80%. The first test was performed with a pooled cDNA sample containing equal portions of cDNA made from all four mouse groups (ND NT, DB NT, ND SKO and DB SKO), the second was performed with diabetic SKO mouse cDNA, and then a third test was performed with a nondiabetic NT mouse cDNA. It was decided that since it failed the primer efficiency using the pooled sample, then again with the specific groups, and that there was nothing found in the literature about the different variances for IRF-1, the RNA may be too low to detect and the primer would not be used.

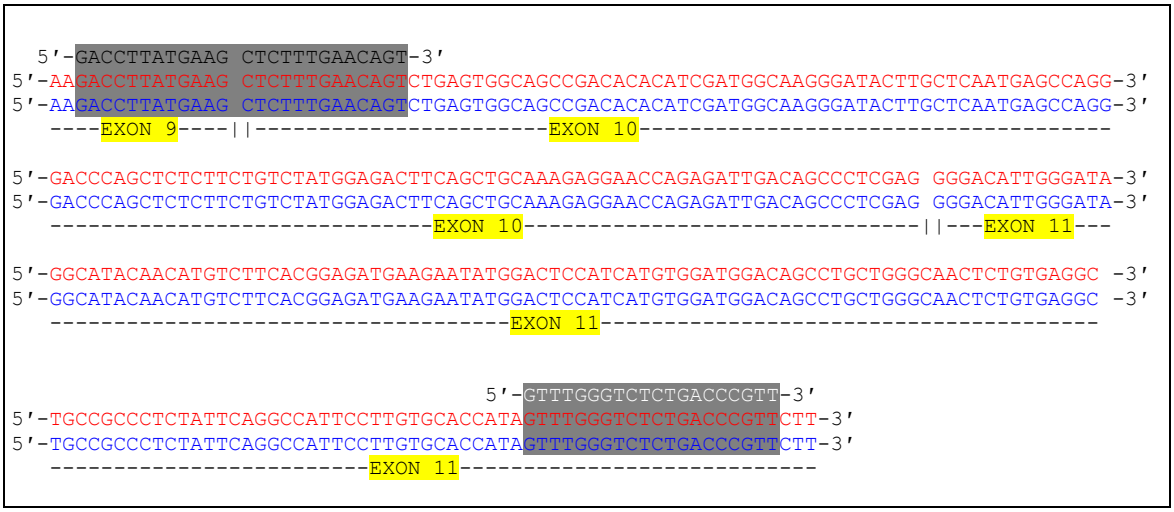

Figure 9. Alignment of *IRF1* gene positive strand for variant 1 (red) and 2 (blue) with the forward primer (black) and the reverse complement of the reverse primer (white).

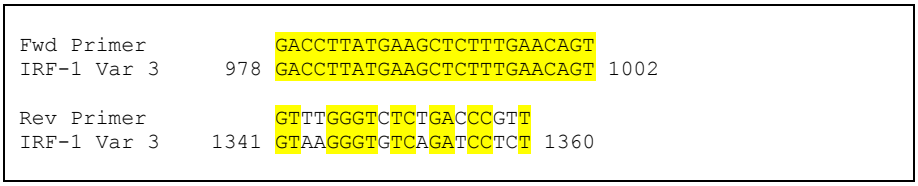

Figure 10. Alignment of *IRF1* variant 3 sequence with *IRF1* v1,2 primers

The primers of *IRF1* var 1,2 exhibited an amplification efficiency of 94.6% (Fig. 11A). Melt curve analysis revealed a single peak, which indicated that these primers create only one product (Fig. 11B). Efficient amplification resulting in a single, specific product was needed since SYBR Green, used for quantitation in the real time reactions, intercalates into any double-stranded DNA and cannot distinguish specific from nonspecific products. Electrophoresis of the real time PCR products on a 2% agarose gel confirmed that the amplified products were similar to the predicted size of 301 bp, demonstrating amplification of variants 1 and 2 (Fig. 12). These tests indicated that the *IRF1* var 1,2 primers were suitable for use in real-time RT-PCR analyses of *IRF1* variant 1 and 2 RNA expression.

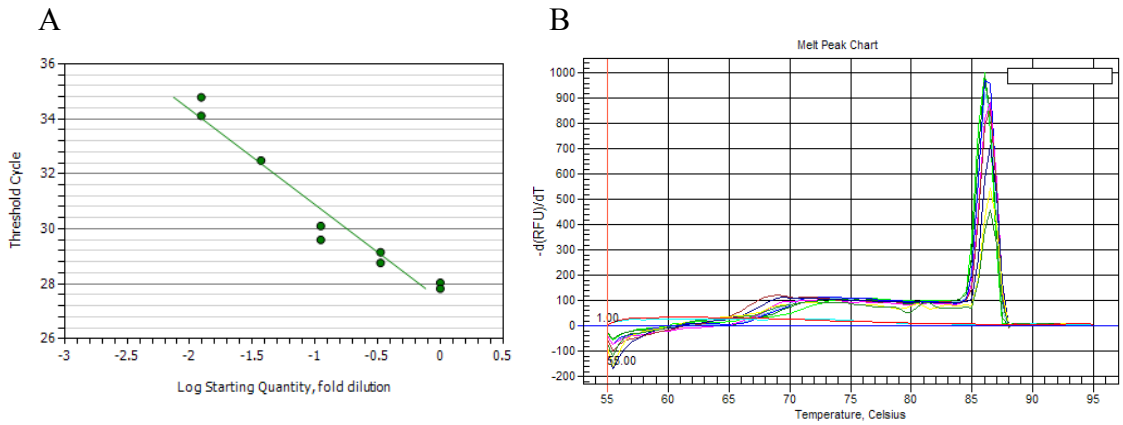

Figure 11. Primer efficiency analysis (A) and melt curve peak chart (B; -dF/dt vs T) for IRF-1 1,2 (+/-) primers.

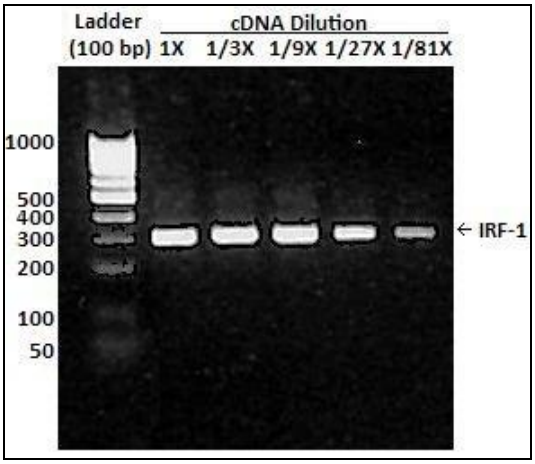

Figure 12. Electrophoresis of IRF-1 primer efficiency real time RT-PCR products.

The closest IRF family member relative to IRF-1 is IRF-2; they share a homologous C-terminal region (Yanai et al., 2012). An alignment was performed between *IRF2* and primer IRF-1 var 1,2,3 (+) and the reverse complement of primer IRF-1 var 1,2 (-) (Fig. 13). This alignment showed a 14 out of 25 nucleotide match between *IRF2* and the forward primer, and 12 out of 20 nucleotide match between *IRF2* and the reverse primer. The product for this, however, is 848 bp; the product seen in the assay is similar to the predicted size of 301 bp, demonstrating that the product is *IRF1* and not *IRF2*.

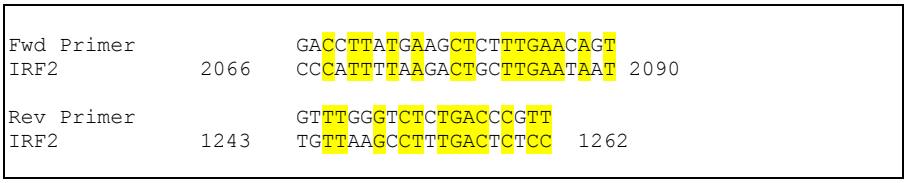

Figure 13. Alignment *IRF2* and *IRF1* v1,2 primers.

4.2 Outlier Identification and Determination of Appropriate Statistical Analyses Methods

Prior to statistical analysis of results for individual experiments, intra-class correlation (ICC) analysis followed by Median Absolute Deviation (MAD) analysis with a critical value of 2.81 was performed in order to identify and remove outliers that might skew interpretation of the results.

Data obtained from experiments assessing IRF1 gene expression were analyzed separately from data of STAT3 experiments in the determination of outliers. First, ICC was performed on results from each assay in order to assess consistency between duplicates, and replicates when applicable; a value greater than 0.70 was considered to be consistent and, hence, reliable data. Western blot analyses of IRF-1, total STAT3 and phosphorylated STAT3 had ICC values below 0.70 prior to the removal of outliers (Table 3, highlighted purple). Results from these western analyses were excluded from the MAD calculations.

Table 3

Summary of Statistics of All Assays

Molecule	**Assay**	**ICC with Outliers**	**ICC without Outliers**	**Likelihood Test**
IRF-1	Real Time	0.8431	0.9452	Wouldn't Run
IRF-1	Real Time Rep 1	0.8743	0.7510	0.0002
IRF-1	Real Time Rep 2	0.9249	0.9198	0.0381
IRF-1	Western	0.3644	0.5437	0.5767
TSTAT3	Western	-0.0791	-0.0846	<0.0001
PSTAT3	Western	-0.0926	-0.0907	<0.0001
TSTAT3	Milliplex	0.9993	0.9951	0.1000
PSTAT3	Milliplex	0.9750	0.9707	0.2090

MAD is considered to be a robust approximation of the commonly used z-score (Upton & Cook, 2008). The critical value of 2.81 was chosen so that observations with scores above the 99.75th percentile and below the 0.25th percentile would be excluded from further analysis since these extreme observations did not belong to the same population as the rest.

MAD analysis with a critical value of 2.81 identified four outlier mice for the IRF-1 experiments and two outlier mice for the STAT3 experiments (Table 4). After removal of the outliers, each IRF-1 assay had an N of 6-10 mice per group and each STAT3 assay had an N of 9-10 mice per group. As stated in the Methods and Materials Section, Mouse 179 was excluded from all protein assays due to not having enough kidney to create a protein lysate. This means that there were only two calculated outliers for STAT3 but there were 3 mice missing. IRF-1 had mouse 179 as a calculated outlier; therefore, the missing mouse does not have an effect (Table 4).

ICC analyses were repeated for all of the assays after removal of outliers to reassess consistency between duplicates, and replicates when applicable. Once again, all

assays except the western blot analyses of IRF-1, total STAT3 and phosphorylated STAT3 had ICC values above 0.70 (Table 3, values below 0.70 highlighted purple).

Table 4

Outlier Mouse Summary

Genotype	Diabetic State	Molecule	Final MAD Score
SKO	ND	IRF-1	6.45
SKO	ND	IRF-1	7.41
SKO	ND	IRF-1	34.75
SKO	DB	IRF-1	5.42
NT	DB	STAT3	5.25
SKO	DB	STAT3	7.12

In order to improve statistical models when needed, a Likelihood test was performed to determine if adding duplicates as a random factor improved the model; if the p value was less than 0.05, then ANOVA and FLSD were performed including duplicates as a random factor to improve the statistical model (Table 3, highlighted blue). The Likelihood test would not run for the combined *IRF1* real time RT-PCR replicate assays. After consultation with Dr. Nakazawa, a Likelihood test was not run for this dataset due to creation of non-divergence by the high ICC values. Statistical analyses were performed separately for each replicate experiment to determine if the two plates would have similar results. Both plates were found to have the same results. Replicate (rep) 1 (Plate 1) had an ICC of 0.751 and rep 2 (Plate 2) had an ICC of 0.920. The Likelihood tests for each replicate had p values less than 0.05; therefore, the duplicates' random factor was included in the statistical analyses for each.

4.3 Analysis of IRF-1 Expression by Real Time RT-PCR

While the name STAT implies an activating role, a repressive role was previously described for STAT5 in the transcriptional regulation of the IRF-1 gene in COS-1 cells

(Luo & Yu-Lee, 2000). STAT5 was shown to competitively inhibit NFκB transcriptional activation of the *IRF1* gene. Thus, using IRF-1 as an example, the objective of this assay was to determine if the expression of IRF-1 RNA is repressed by STAT5 in the kidney, or, more precisely, if expression of IRF-1 RNA is increased in the absence of STAT5 in the kidney, which would imply a repressive role for STAT5 in the kidney.

Real time RT-PCR was performed to determine the relative expression of *IRF-1* RNA in the kidney in the presence and absence of STAT5 and diabetes. Duplicate reactions were analyzed for each kidney sample within a single plate and the real time analysis was performed twice (replicated) on separate plates. *IRF1* RNA expression was significantly increased in the DB SKO mice when compared to the ND SKO group and the DB NT group (Fig. 14). *IRF1* RNA expression was also significantly increased when comparing the ND SKO group to the ND NT group (Fig. 14). *IRF1* RNA expression did not differ significantly when comparing the DB NT group with the ND NT group. The results for the separate replicates (Fig. 15) reflected the results when both replicates were analyzed together (Fig. 14), suggesting that a single real time experiment performed with duplicate reactions for each sample would have been sufficient to reach statistical significance.

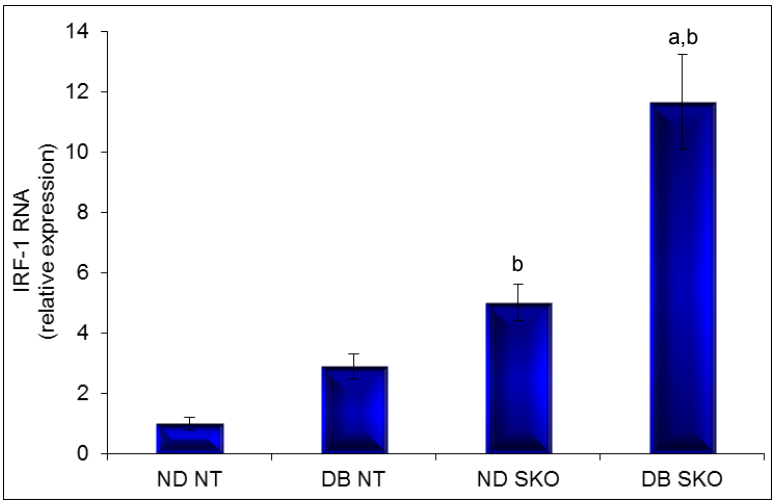

Figure 14. *IRF1* real time RT-PCR results. ND, non-diabetic; DB, diabetic; NT, non-transgenic or wild-type; SKO, STAT5A/B knockout. a = significantly different ($p<0.05$) from ND counterpart. b = significantly different ($p<0.05$) from NT counterpart

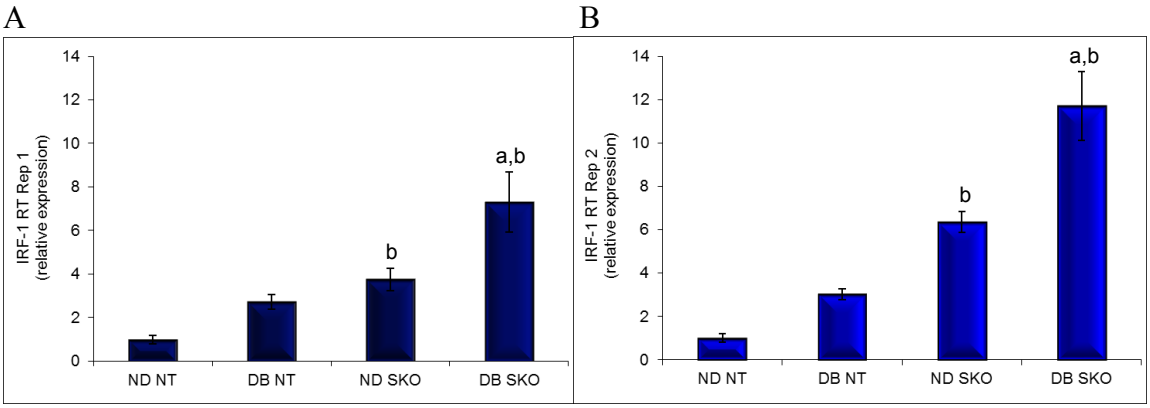

Figure 15. IRF1 real time RT-PCR results for Replicate 1 (A) and Replicate 2 (B). a = significantly different ($p<0.05$) from ND counterpart. b = significantly different ($p<0.05$) from NT counterpart.

Electrophoresis of the amplified real time PCR products from the first two mice of each group of replicate 1 on a 2% agarose gel confirmed that the amplified products were similar to the predicted size of 301 base pairs (Fig. 16).

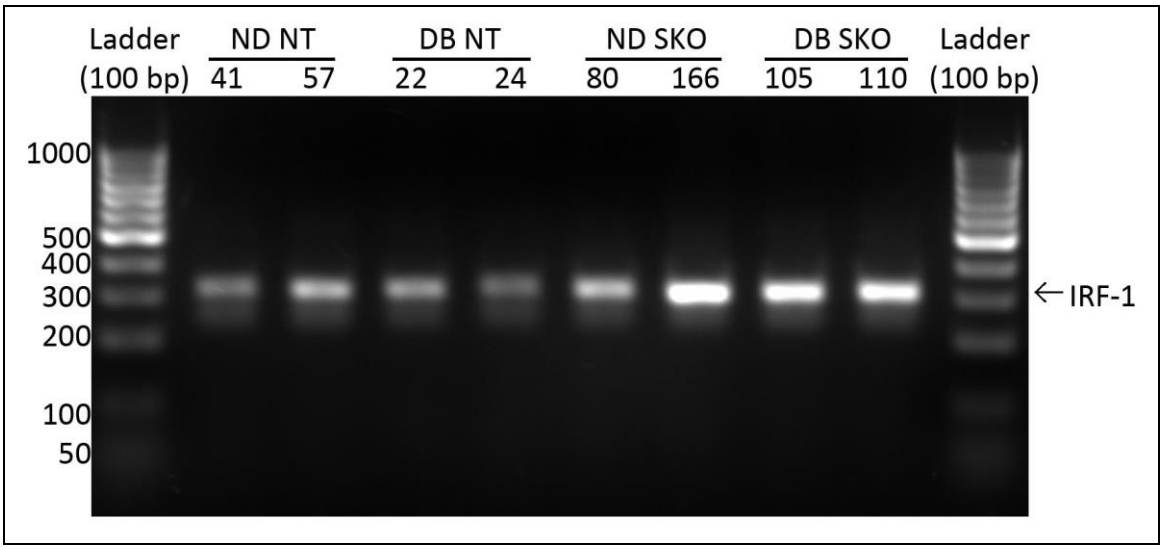

Figure 16. Electrophoresis of the amplified *IRF1* Real Time PCR products from the first two mice of each group.

4.4 IRF-1 Western Blot Analysis

Relative IRF-1 protein expression was examined by western blot analysis of kidney protein lysates. A pattern similar to IRF-1 RNA expression was expected since

others had shown that the level of IRF-1 protein appears to correspond with the level of IRF-1 RNA expression (Kroger et al., 2002). Further, an increase of IRF-1 protein might help explain the increase in *VCAM1* gene expression that is seen (Coschigano et al., unpublished data), since IRF-1 and NFκB are the main transcription factors for VCAM-1. A single band of the expected size (~48 kDa) was seen for IRF-1; a specific band (~42kDa), as well as several nonspecific bands, was observed for the β-actin loading control (Fig. 17, bottom panel). An ICC below the level of significance was calculated for the western analyses of IRF-1; therefore, no conclusions regarding differences in IRF-1 protein expression between the four mouse groups could be drawn.

4.5 Western Blot Analyses of Phosphorylated and Total STAT3 Protein

In the absence of STAT5, many inflammation-related genes are upregulated in the diabetic SKO mice. It has previously been shown in hepatocytes and liver tissue that STAT3 phosphorylation increases in the absence of STAT5 (Cui et al., 2007). It has also been shown that phosphorylated STAT3 induces the expression of inflammation-related genes (Grivennikov & Karin, 2010; Yang et al., 2007). Furthermore, increased levels of phosphorylated STAT3 can lead to increased levels of unphosphorylated STAT3, which in turn activate NFκB, leading to increased expression of inflammation-related genes (Grivennikov & Karin, 2010; Yang et al., 2007). Thus, in the current study, the levels of phosphorylated and unphosphorylated STAT3 were assessed to determine if increased inflammation-related gene expression might be due to an increase in phosphorylated and/or unphosphorylated STAT3 activity in the kidney in the absence of STAT5.

Western blot analysis was performed to determine the relative protein levels of phosphorylated STAT3 in kidney protein lysates. Bands that appeared to correspond to phosphorylated versions of the two isoforms of STAT3, STAT3α (86 kDa) and STATβ (79 kDa) (Biethahn, Alves, Wilde, Hiddemann, & Spiekermann, 1999), were observed (Fig. 17). An ICC below the level of significance was calculated for the western analyses of phosphorylated STAT3; therefore, no conclusions regarding differences in expression between the four groups could be drawn.

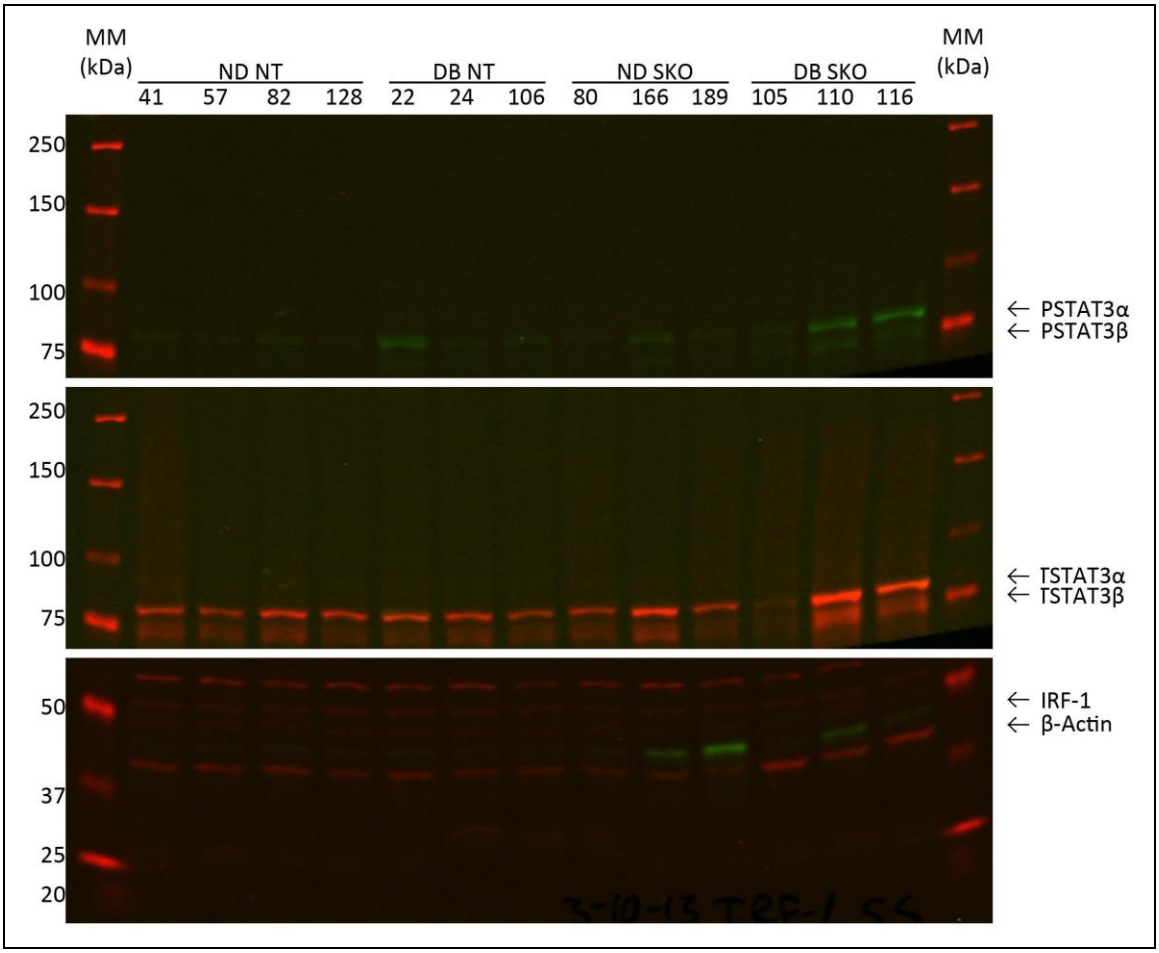

Figure 17. A representative western blot image of phosphorylated STAT3 (green, top panel), total STAT3 (red, center panel), IRF-1 (green, bottom panel), and β-actin (red, bottom panel) protein expression. All images were obtained from a single membrane from a single gel.

Since there is no antibody specific for unphosphorylated STAT3, western blot analyses of the same gels assayed for phosphorylated STAT3 were also performed to determine the protein levels of total STAT3 with the expectation of estimating unphosphorylated STAT3 protein levels based on total and phosphorylated STAT3 protein levels (Yue et al., 2010). Bands that appeared to correspond to the two isoforms of STAT3, STAT3α (86 kDa) and STAT3β (79 kDa) (Biethahn et al., 1999), were observed (Fig. 17). However, as seen for the previous western analyses, an ICC below the level of significance was calculated for the western analyses of total STAT3; therefore, no estimates of unphosphorylated STAT3 protein levels could be obtained.

4.6 Milliplex Analyses of Phosphorylated and Total STAT3 Protein Levels

Milliplex magnetic bead assays were performed in an attempt to quantify and compare phosphorylated and total STAT3 protein levels in the kidney protein lysates. Phosphorylated STAT3, total STAT3, and β-tubulin signals from the kidney samples fell within the linear region of curves that were made from titration of the positive controls.

Phosphorylated STAT3 protein levels were significantly increased in the DB SKO group when compared to the ND SKO group and the DB NT group (Fig. 18A). There were no significant differences when comparing the ND SKO and the ND NT groups or the DB NT and the ND NT groups.

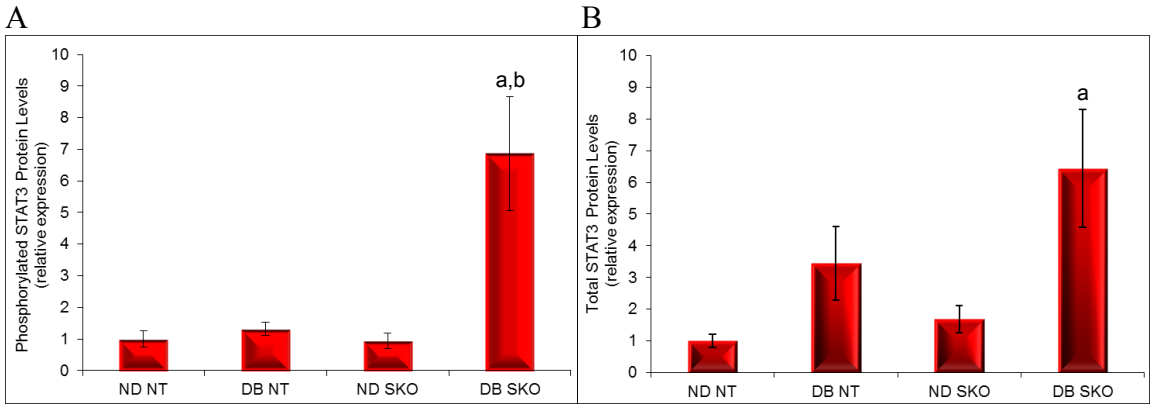

Figure 18. Milliplex magnetic bead assay of phosphorylated STAT3 (A) and total STAT3 (B) protein levels. a = significantly different ($p<0.05$) from ND counterpart. b = significantly different ($p<0.05$) from NT counterpart.

Total STAT3 protein levels also were significantly increased when comparing the DB SKO group to the ND SKO group (Fig. 18B). Although not reaching statistical significance, there was a trend (p value = 0.051) for increased expression of the DB SKO group in comparison to the DB NT group. There was no significant difference between the ND SKO and ND NT groups or between the DB NT and ND NT groups.

Since an assay specific for unphosphorylated STAT3 is unavailable, total STAT3 and phosphorylated STAT3 levels were compared in order to approximate the levels of

unphosphorylated STAT3. No significant differences in the approximated levels of unphosphorylated STAT3 were found between any of the groups (Fig. 19).

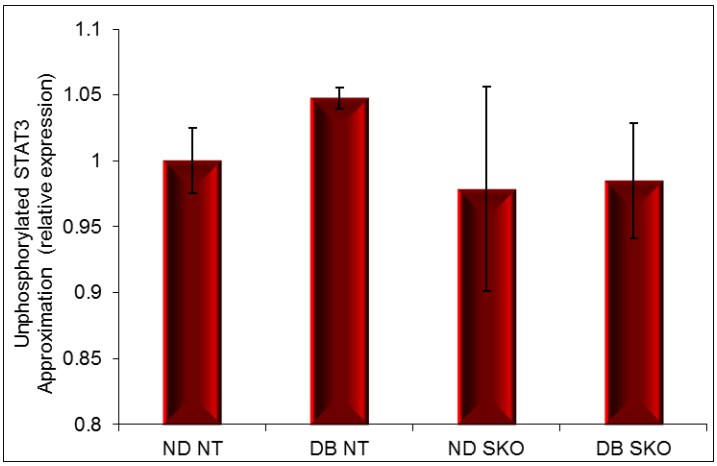

Figure 19. Approximation of unphosphorylated STAT3 protein levels.

CHAPTER 5: DISCUSSION

The central hypothesis of this thesis was that the combination of the loss of STAT5 repression and increase of STAT3 activity escalates inflammation-related gene expression in the kidneys of diabetic STAT5A/B knockout mice. This hypothesis was tested by two specific aims. Specific Aim I tested the repressive function of STAT5 and Specific Aim II tested the activation of STAT3 in the absence of STAT5.

5.1 Outlier Justification

After a statistical test would not run for the real time analysis, it was found that the data set had an outlier that would not allow some of the multilevel models to converge. All data sets were then examined for outliers. An outlier is defined as a value that diverges extremely from the other values of the same group (Grubbs, 1969; Hodge & Austin, 2004). Further, an outlier can also be defined as a value that seems to be inconsistent with the rest of the group (Hodge & Austin, 2004). A statistical test is used to determine outliers (Hodge & Austin, 2004). A test is chosen; the score is calculated and is then compared to a critical value with a low significance level (Grubbs, 1969). After consultation with Dr. Masato Nakazawa, the HCOM Biostatistician, Median Absolute Deviation (MAD) was selected to calculate outliers.

Four mice were found to be outliers when examining IRF-1 RNA levels. A possible reason for the outliers for IRF-1 is that the housing created stress. Mice are social creatures and typically group housed up to four per cage in our facility, unless there is fighting. Mouse 189 and 179 with the two highest MAD scores were singly housed, which may have caused stress. Prolactin is secreted during stressful times (Khansari, Murgo, & Faith, 1990). IRF-1 has been shown to be increased by prolactin in granulocytes (Hooghe, Dogusan, Martens, Velkeniers, & Hooghe-Peters, 2001). Thus, the stress may have resulted in abnormal secretion of prolactin and aberrant levels of IRF-1. Furthermore, when males are housed together a social hierarchy is determined and maintained by fighting (Brown, 1953). It was also seen that dominant mice would take

food forcibly from the subordinate mice (Brown, 1953). Mouse 166 had the next highest score; upon further investigation it was found that he was housed with three other mice but they were NT mice. Mouse 166 was the smallest of this cage. Mouse 148, the fourth outlier, was group housed with another SKO and one NT. It is possible that the size differences between the SKO and NT mice made that worse for the aforementioned mice. This could cause a stressful environment.

Another possible explanation for the outlier mice is that they could have had an infection or possible damage that was not detectable to the naked eye. Both STAT3 and IRF-1 are activated by a wide variety of cytokines (Grivennikov & Karin, 2010; Kroger et al., 2002). Cytokines are proteins that are released by cells that affect the activities of other cells and are used to recruit other cells to sites of infection and damage (Moser & Leo, 2010). It is possible that cytokine levels in the outlier mice were high due to reasons unrelated to the specific diabetes study, causing significant deviation from the group of mice as a whole. Cytokine levels could be measured in a variety of assays, such as an ELISA, a western blot analysis, or a Milliplex magnetic bead assay, in order to test this theory.

5.2 Repressive Function of STAT5

The working hypothesis that specific aim I tested was that the loss of STAT5 repression of NFκB transcriptional activity in the kidney would result in a significant increase of IRF-1 RNA, which in turn should lead to a significant increase in IRF-1 protein (Fig. 14). This hypothesis was based on the previous observation that PRL-induced STAT5B inhibits transcription of the *IRF1* gene by NFκB and STAT1 (Luo & Yu-Lee, 2000; Yu-Lee, 2001).

In the current study, RNA expression was assayed by real time RT-PCR to see if the transcription of the *IRF1* gene would be increased in diabetic mouse kidneys in the absence of STAT5 and its presumed repressive function. No significant increase in *IRF1* RNA expression was seen with just the induction of diabetes. However, there was an

increase in *IRF1* RNA expression seen with just the absence of STAT5 and an even greater increase with the induction of diabetes in the absence of STAT5.

IRF1 RNA expression did support a possible inhibitory role of NFκB by STAT5 in the kidney, since *IRF1* RNA expression was increased in the absence of STAT5. The further increase of *IRF1* RNA expression with the combination of diabetes in the absence of STAT5 suggested further relief of transcriptional inhibition, but the mechanism is unclear. IRF-1 mRNA levels accrue in response to certain hormones, double-stranded RNA, interferon, retinoic acid, developmental cues, and certain cytokines (Kroger et al., 2002; Yu-Lee, 2001). Cytokines released during diabetic nephropathy could activate *IRF1* gene transcription, further increasing the levels of *IRF1* and explaining the even greater increase in *IRF1* RNA expression with the combination of the absence of STAT5 and presence of diabetes.

The *IRF1* gene is also regulated by STAT1 ((Luo & Yu-Lee, 2000). It has been shown in hepatocytes and liver tissue that there is an increase of phosphorylated STAT1 levels in the absence of STAT5 (Cui et al., 2007). Thus, another possible reason for the *IRF1* mRNA increase in the SKO kidneys could be due to an increase in STAT1 activity rather than a loss of limiting cofactor sequestration in the absence of STAT5. Phosphorylated STAT1 protein levels were not assessed in kidneys of these mice. Phosphorylated STAT1 protein levels could be determined with enzyme-linked immunosorbent assay (ELISA), milliplex, or a western blot analysis. These results could help establish whether an increase in STAT1 may contribute to the increase in *IRF1* RNA that was seen.

There were three *IRF1* variants found when searching the nucleotide database of NCBI (http://www.ncbi.nlm.nih.gov/nuccore), variant 1 (NM_008390.2), variant 2 (NM_001159396.1), and variant 3 (NM_001159393.1). According to the NCBI website (http://www.ncbi.nl m.nih.gov/gene/?term =NM_001159396.1), *IRF1* variants 1 and 2 encode an identical protein product (NP_001152865.1). *IRF1* variant 3 encodes a different protein product (NP_001152865.1). With a literature search that found nothing about these *IRF1* variants or their protein products and that *IRF1* variant 3 failed three different primer efficiency tests, it was decided to not test for the *IRF1* variant 3. The

significant results found for the first two variants of the *IRF1* gene does support the possible inhibitory role of NFκB by STAT5 in the kidney but would variant 3? Primers could be redesigned to determine if it was the primers that failed or is there just no variant 3 in the groups.

IRF-1 protein levels were assessed to help explain the previous finding of increased VCAM-1 expression (Coschigano et al., unpublished data). The mRNA levels of IRF-1 were expected to reflect the levels of protein since the protein only has a half-life of thirty minutes (Kroger et al., 2002). In the current study, no conclusive results regarding differences in IRF-1 protein expression between the four groups could be drawn due to inconsistencies of the duplicates within the western analyses reflected by the ICC value. This could have been due to the semi-quantitative nature of western blot analyses or the signal not being strong enough. The short half-life of the protein suggests that the latter was likely to be the case. A more sensitive measure of IRF-1 protein is probably needed to address this issue, such as an ELISA specific for IRF-1.

5.3 STAT3 Activation in the Absence of STAT5

The working hypothesis that specific aim II tested was that there would be a significant increase in levels of phosphorylated STAT3 protein as a result of the absence of STAT5 that could in turn account for the increase in inflammation-related gene expression. The basis for this hypothesis was that, in the absence of STAT5, an increase of phosphorylated STAT3 in hepatocytes and liver tissue has been observed (Cui et al., 2007). The Milliplex magnetic bead assay demonstrated a significant increase in phosphorylated STAT3 protein levels in the absence of STAT5, but only when the mice were diabetic. In contrast to the literature, which showed increased levels of phosphorylated STAT3 in diabetic wildtype mice (Lu et al., 2009); there was no significant difference in phosphorylated STAT3 levels between the diabetic and non-diabetic non-transgenic mouse groups in the current study. The published study differs from the current study in that phosphorylated levels of STAT3 were investigated specifically in glomeruli of the mice (Lu et al., 2009), while the current study used

protein lysates isolated from the whole kidney. It is possible that a significant increase in phosphorylated STAT3 in the glomeruli was reduced to insignificance when extracting protein from the whole kidney if this difference was not evident in other regions of the kidney as well.

A possible mechanism explaining the increase in phosphorylated STAT3 in the absence of STAT5 and presence of diabetes starts with the loss of repression of NFκB by STAT5B (Fig. 20). NFκB then activates the transcription of IL-6 (Yang et al., 2007). As stated previously STAT3 is activated by IL-6, a proinflammatory cytokine that has also been linked to diabetic complications such as DN, making STAT3 an important mediator for DN (Lu et al., 2009). If the transcription of IL-6 is indirectly repressed by STAT5B, then STAT3 will not be activated and therefore there will be no increase seen in the diabetic mice with intact STAT5 genes.

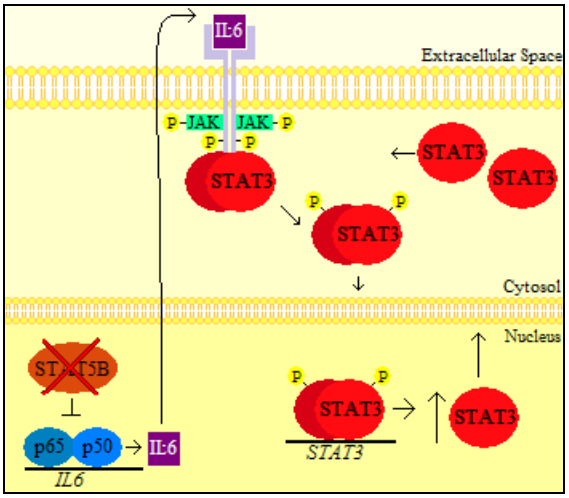

Figure 20. Possible effect on STAT3 when STAT5B inhibition of NFκB is removed.

To try to test the effect of the loss of STAT5 without subsequent activation of STAT3, a STAT3 25% activity mouse (Lu et al., 2009) could be bred with the STAT5 hypomorph mouse, creating a STAT3 25%/STAT5 hypomorph mouse line. After the induction of diabetes in this line and harvesting of kidneys, a mircoarray analysis or real time RT-PCR could be performed for inflammation-related genes that are currently found to be increased. These results could be compared to the individual knockouts. If the

inflammation-related genes are not increased in the absence of STAT5A/B and reduction of STAT3, then increased activity of STAT3 in the absence of STAT5A/B is likely causing the increased expression of the inflammation-related genes in the current study.

Activation of phosphorylated STAT3 by IL-6 also leads to an increase in unphosphorylated STAT3 (Jamieson et al., 2012; Yang et al., 2005; Yang et al., 2007). This was found specifically in kidney and spleen tissue (Narimatsu et al., 2001). Unphosphorylated STAT3 in turn can activate NFκB as was demonstrated in hTERT-HME1 cells (Fig. 16) (Grivennikov & Karin, 2010; Yang et al., 2007). NFκB p65 subunit binding activity was found to be increased in the diabetic SKO animals.

There was no Milliplex assay for unphosphorylated STAT3, so the Milliplex assay for total STAT3 was performed in the current study and unphosphorylated STAT3 levels were approximated by subtracting the ratio of phosphorylated STAT3 levels to total STAT3 levels from a value of one. The approximated unphosphorylated STAT3 levels showed no significant differences between any of the groups. This too conflicted with the literature; it was expected that an increase of phosphorylated STAT3 in the diabetic STAT5 knockout mice would lead to an increase of unphosphorylated STAT3 in the same mice.

A possible explanation for the conflict between expected results and the approximated values is that phosphorylated STAT3 is so in demand in the diabetic SKO mice that the unphosphorylated STAT3 is phosphorylated as quickly as it is translated; therefore there was no increased unphosphorylated STAT3 in the cytoplasm to be detected. Another possible explanation was that the approximation itself was not reliable enough to detect the differences in unphosphorylated STAT3. If this is the case unphosphorylated STAT3 would need to be directly measured. This is difficult as no Milliplex magnetic bead assay is available and no antibody to unphosphorylated STAT3 is commercially available. One way to measure unphosphorylated STAT3 is to have an antibody created that recognizes only unphosphorylated STAT3. Another way could be to use a total STAT3 antibody in a western blot analysis with a gradient gel that would separate the phosphorylated and the unphosphorylated forms, the latter being a slightly smaller molecular weight.

Unphosphorylated STAT3 protein levels could be determined by creating an antibody that recognizes the unphosphorylated 705 tyrosine that could then be utilized in immunoprecipitation, ELISA, or western blot analysis. These results could support the literature that an increase in phosphorylated STAT3 leads to an increase of unphosphorylated STAT3 (Jamieson et al., 2012; Yang et al., 2005; Yang et al., 2007).

Western blot analysis was also attempted for comparison of phosphorylated and total STAT3 levels in kidneys of the various mouse groups. Western blot analysis can be used to assess multiple proteins at a time, either by stripping the membrane and reprobing or by using secondary antibodies that are labeled with two different colored dyes. The membranes for this analysis can be stored for weeks and possibly reprobed again to look for other proteins. But western blot analyses are only semi-quantitative and may have high background. If high background or low specific signal persists, an alternative antibody could be tried if available. In the current study, no significant differences could be found because of the inaccuracy of quantification due to the inability of the results to be duplicated, which is reflected by the ICC value.

Duplication may not have been possible due to a weak signal of the protein. What the westerns did show was two STAT3 isoforms (doublet band) at the expected molecular weights. The STAT3 isoforms are generated through alternative mRNA splicing, STAT3α (94 kDa) and STAT3β (83 kDa) (Biethahn et al., 1999; Huang et al., 2007). STAT3β is missing the C-terminal acidic transactivation domain found in STAT3α, instead replaced by seven unique amino acid residues (CT7 domain) (Huang et al., 2007). The presence of both STAT3 isoforms raises the question of what role each has in the kidney.

It has been shown that the isoforms have distinct and overlapping functions in pathophysiology, normal biology, and gene transcription (Huang et al., 2007). Both isoforms are phosphorylated at tyrosine 705 and form homodimers and heterodimers with STAT1 (Schaefer, Sanders, Park, & Nathans, 1997). It was shown in COS-7 cells that STAT3α has a greater transcriptional activity but STAT3β has a greater binding affinity (Schaefer et al., 1997).

In previous experiments it was shown that, in contrast to the embryonic lethality of mice lacking both STAT3α and STAT3β, mice deficient in STAT3α but still producing STAT3β were born but died within 24 hours of birth showing that the β isoform was sufficient to get the mice to the neonatal stage but the α isoform was needed for further survival (Maritano et al., 2004). Mice deficient in STAT3β did not experience lethality showing that STAT3β is not essential for viability (Maritano et al., 2004). These mice were also found to be hypersensitive to lipopolysaccharide, which was used to induce inflammation, with an upregulation of inflammation-related genes. Mice deficient in STAT3α, while still having STAT3β, produced significantly less TNF and IL-6 than the STAT3 knockout mice lacking both isoforms, showing that STAT3β has a negative effect on inflammatory cytokine synthesis (Maritano et al., 2004).

The Milliplex assay cannot distinguish between the two phosphorylated isoforms as it, like the western blot antibody, recognizes phosphorylation of the 705 tyrosine residue common to both isoforms. Therefore, the increase of phosphorylated STAT3 seen in the Milliplex assay cannot be attributed to one isoform over the other and, thus, it cannot be determined which activity predominates. If STAT3β protects against inflammation, it is possible that the upregulation in phosphorylated STAT3 is due to the upregulation of STAT3β in response to or as a result of the increase in inflammation-related genes, rather than as a cause of the increase.

Western blot analyses could be attempted with higher protein concentration to compare the protein levels for each STAT3 isoform. The westerns separate proteins according to size; this could be done with the current antibodies and quantitating each band separately. An ELISA could also be created utilizing antibodies raised against the unique C-terminal regions of each isoform. These results would help elucidate which STAT3 isoform and associated activity predominates in the kidney of each test group.

Using cell culture is another way to determine the activities of each STAT3 isoform. Renal cells in culture could be stimulated with a known activator of STAT3 and siRNA for each isoform could be introduced to separate cultures of the cells. Real time RT-PCR could then be performed on RNA from each separate cell culture for the

previous inflammation-related genes found to be upregulated. These results then could be compared and the activity of each isoform could be elucidated.

5.4 Conclusion

Inflammation-related genes are upregulated in diabetic STAT5A/B knockout mice (Coschigano et al., unpublished). One possible mechanism for this upregulation, relief of the repression of NFκB by STAT5, was supported by the observed increase in *IRF1* RNA expression in diabetic STAT5A/B knockout mice, which served as a model system for testing this mechanism (Fig. 21). A second possible mechanism for the upregulation of inflammation-related genes, activation of STAT3 in the absence of STAT5, was also supported by observation of increased phosphorylated STAT3 in the diabetic STAT5A/B knockout mice (Fig. 21). NFκB is associated with increased transcription of genes encoding cytokines, chemokines, inhibitors of apoptosis, and enzymes that produce secondary inflammatory mediators and adhesion molecules (Bonizzi & Karin, 2004), while STAT3 is a regulator of immune response genes, such as cytokines and inflammatory/immune mediators (Grivennikov & Karin, 2010; Lu et al., 2009).

While the hypothesis has support, further validation is still required. The possibility that an increase in STAT1 could contribute to the increased *IRF1* RNA expression needs to be addressed. Determining IRF-1 protein levels needs to be done to tie the repressive role of STAT5B to VCAM-1 expression. Unphosphorylated STAT3 needs to be directly measured instead of approximated to truly determine if changes in its levels may be playing a regulatory role. The STAT3 protein isoform levels need to be determined to elucidate a possible protective role for STAT3β.

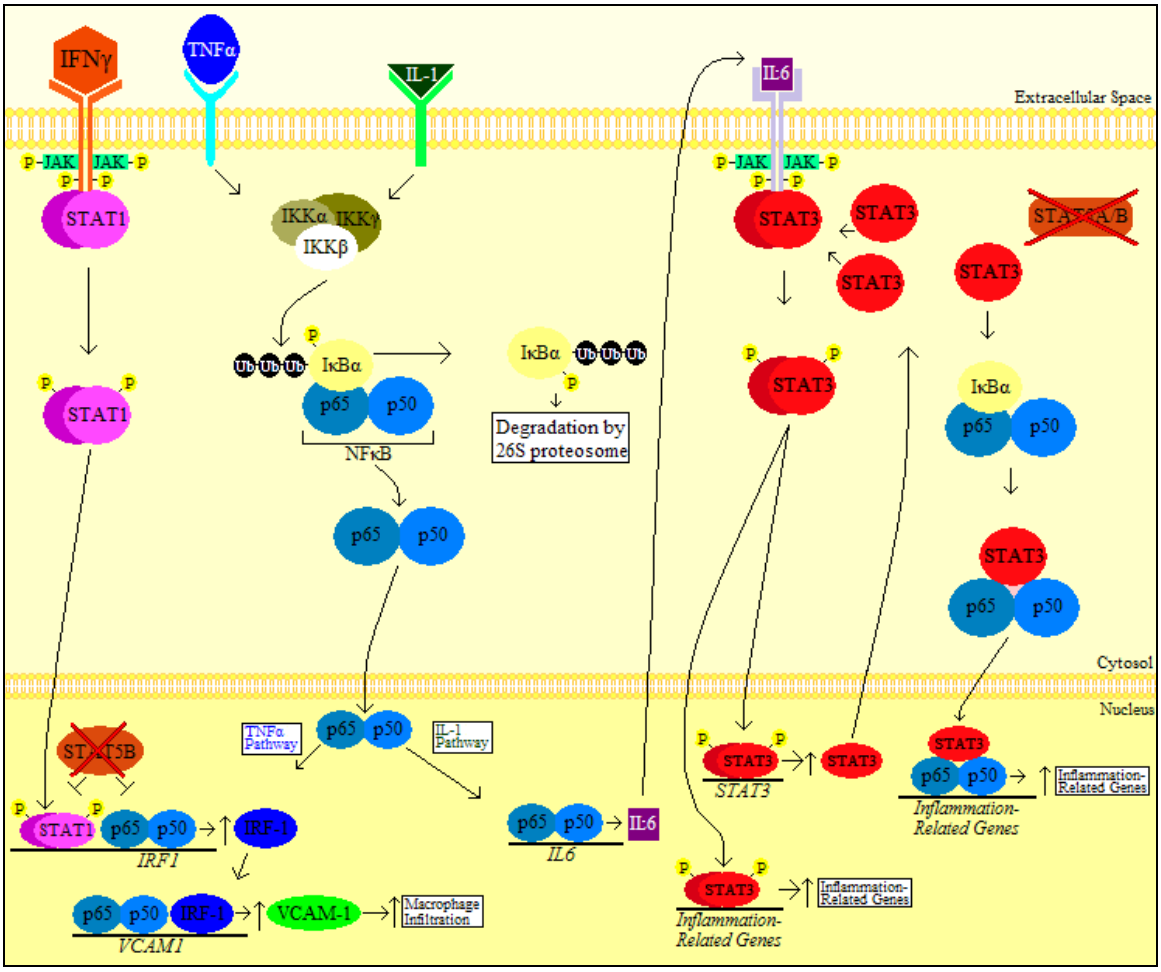

Figure 21. Possible effects of the absence of the STAT5A/B proteins.

REFERENCES

American Diabetes Association. (2012). Diagnosis and classification of diabetes mellitus. *Diabetes Care, 35*, S64-S71.

American Diabetes Association. (2014). *DKO (ketoacidosis) & ketones.* Retrieved 04-10-14, 2014, from http://www.diabetes.org/living-with-diabetes/complications/ketoacidosis- dka.html

Andersen, C. L., Jensen, J. L., & Orntoft, T. F. (2004). Normalization of real-time quantitative reverse transcription-PCR data: A model-based variance estimation approach to identify genes suited for normalization, applied to bladder and colon cancer data sets. *Cancer Research, 64*(15), 5245-5250.

Atkinson, M. A., & Skyler, J. S. (2012). Type 1 diabetes. In J. S. Skyler (Ed.), *Atlas of diabetes: Fourth edition* (pp. 65-94) Springer.

Baldwin, A. S.,Jr. (1996). The NF-kappa B and I kappa B proteins: New discoveries and insights. *Annual Review of Immunology, 14*, 649-683.

Biethahn, S., Alves, F., Wilde, S., Hiddemann, W., & Spiekermann, K. (1999). Expression of granulocyte colony-stimulating factor- and granulocyte-macrophage colony-stimulating factor-associated signal transduction proteins of the JAK/STAT pathway in normal granulopoiesis and in blast cells of acute myelogenous leukemia. *Experimental Hematology, 27*(5), 885-894.

Bonizzi, G., & Karin, M. (2004). The two NF-kappaB activation pathways and their role in innate and adaptive immunity. *Trends in Immunology, 25*(6), 280-288.

Brosius, F. C.,3rd. (2008). New insights into the mechanisms of fibrosis and sclerosis in diabetic nephropathy. *Reviews in Endocrine & Metabolic Disorders, 9*(4), 245-254.

Brown, R. Z. (1953). Social behavior, reproduction, and changes in house mouse (*mus musculus* L.). *Ecol Monogr, 23*, 217-240.

Buitenhuis, M., Coffer, P. J., & Koenderman, L. (2004). Signal transducer and activator of transcription 5 (STAT5). *The International Journal of Biochemistry & Cell Biology, 36*(11), 2120-2124.

Centers for Disease Control and Prevention. (2011). *National diabetes fact sheet: National estimates and general information on diabetes and prediabetes in the united states, 2011*. Atlanta, GA: U.S. Department of Health and Human Services, Centers for Disease Control and Prevention.

Collins, T., Read, M. A., Neish, A. S., Whitley, M. Z., Thanos, D., & Maniatis, T. (1995). Transcriptional regulation of endothelial cell adhesion molecules: NF-kappa B and cytokine-inducible enhancers. *FASEB Journal : Official Publication of the Federation of American Societies for Experimental Biology, 9*(10), 899-909.

Cui, Y., Hosui, A., Sun, R., Shen, K., Gavrilova, O., Chen, W., et al. (2007). Loss of signal transducer and activator of transcription 5 leads to hepatosteatosis and impaired liver regeneration. *Hepatology (Baltimore, Md.), 46*(2), 504-513.

Cui, Y., Riedlinger, G., Miyoshi, K., Tang, W., Li, C., Deng, C. X., et al. (2004). Inactivation of Stat5 in mouse mammary epithelium during pregnancy reveals distinct functions in cell proliferation, survival, and differentiation. *Molecular and Cellular Biology, 24*(18), 8037-8047.

Eroschenko, V. P. (2008). *diFiore's atlas of histology with functional correlations* (11th ed.). Philadelphia, PA: Lippincott Williams & Wilkins.

Grivennikov, S. I., & Karin, M. (2010). Dangerous liaisons: STAT3 and NF-kappaB collaboration and crosstalk in cancer. *Cytokine & Growth Factor Reviews, 21*(1), 11-19.

Grubbs, F. E. (1969). Procedures for detecting outlying observations in samples. *Technometrics, 11*, 1-21.

Hayden, M. S., & Ghosh, S. (2008). Shared principles in NF-kappaB signaling. *Cell, 132*(3), 344-362.

Hennighausen, L., & Robinson, G. W. (2008). Interpretation of cytokine signaling through the transcription factors STAT5A and STAT5B. *Genes & Development, 22*(6), 711-721.

Hodge, V. J., & Austin, J. (2004). A survey of outlier detection methodologies. *Artif Intell Rev, 22*, 85-126.

Hooghe, R., Dogusan, Z., Martens, N., Velkeniers, B., & Hooghe-Peters, E. L. (2001). Effects of prolactin on signal transduction and gene expression: Possible relevance for systemic lupus erythematosus. *Lupus, 10*(10), 719-727.

Huang, Y., Qiu, J., Dong, S., Redell, M. S., Poli, V., Mancini, M. A., et al. (2007). Stat3 isoforms, alpha and beta, demonstrate distinct intracellular dynamics with prolonged nuclear retention of Stat3beta mapping to its unique C-terminal end. *The Journal of Biological Chemistry, 282*(48), 34958-34967.

Ihle, J. N. (2001). The stat family in cytokine signaling. *Current Opinion in Cell Biology, 13*(2), 211-217.

Jamieson, A. M., Farlik, M., & Decker, T. (2012). How stats interact with the molecular machinery of transcriptional activation. In M. Decker, & M. Müller (Eds.), *Jak-stat signaling: From basics to disease* (pp. 65-89) Springer-Verlag Wien.

Kanwar, Y. S., Wada, J., Sun, L., Xie, P., Wallner, E. I., Chen, S., et al. (2008). Diabetic nephropathy: Mechanisms of renal disease progression. *Experimental Biology and Medicine (Maywood, N.J.), 233*(1), 4-11.

Khansari, D. N., Murgo, A. J., & Faith, R. E. (1990). Effects of stress on the immune system. *Immunology Today, 11*(5), 170-175.

Koga, M., Otsuki, M., Kubo, M., Hashimoto, J., & Kasayama, S. (1998). Relationship between circulating vascular cell adhesion molecule-1 and microvascular complications in type 2 diabetes mellitus. *Diabetic Medicine : A Journal of the British Diabetic Association, 15*(8), 661-667.

Kroger, A., Koster, M., Schroeder, K., Hauser, H., & Mueller, P. P. (2002). Activities of IRF-1. *Journal of Interferon & Cytokine Research : The Official Journal of the International Society for Interferon and Cytokine Research, 22*(1), 5-14.

Lim, C. P., & Cao, X. (2006). Structure, function, and regulation of STAT proteins. *Molecular bioSystems, 2*(11), 536-550.

Liu, X., Robinson, G. W., Gouilleux, F., Groner, B., & Hennighausen, L. (1995). Cloning and expression of Stat5 and an additional homologue (Stat5b) involved in prolactin signal transduction in mouse mammary tissue. *Proceedings of the National Academy of Sciences of the United States of America, 92*(19), 8831-8835.

Liu, X., Robinson, G. W., Wagner, K. U., Garrett, L., Wynshaw-Boris, A., & Hennighausen, L. (1997). Stat5a is mandatory for adult mammary gland development and lactogenesis. *Genes & Development, 11*(2), 179-186.

Lu, T. C., Wang, Z. H., Feng, X., Chuang, P. Y., Fang, W., Shen, Y., et al. (2009). Knockdown of Stat3 activity in vivo prevents diabetic glomerulopathy. *Kidney International, 76*(1), 63-71.

Luis-Rodriguez, D., Martinez-Castelao, A., Gorriz, J. L., De-Alvaro, F., & Navarro-Gonzalez, J. F. (2012). Pathophysiological role and therapeutic implications of inflammation in diabetic nephropathy. *World Journal of Diabetes, 3*(1), 7-18.

Luo, G., & Yu-Lee, L. (2000). Stat5b inhibits NFkappaB-mediated signaling. *Molecular Endocrinology (Baltimore, Md.), 14*(1), 114-123.

Luster, A. D., Alon, R., & von Andrian, U. H. (2005). Immune cell migration in inflammation: Present and future therapeutic targets. *Nature Immunology, 6*(12), 1182-1190.

Maritano, D., Sugrue, M. L., Tininini, S., Dewilde, S., Strobl, B., Fu, X., et al. (2004). The STAT3 isoforms alpha and beta have unique and specific functions. *Nature Immunology, 5*(4), 401-409.

Matsui, F., & Meldrum, K. K. (2012). The role of the janus kinase family/signal transducer and activator of transcription signaling pathway in fibrotic renal disease. *The Journal of Surgical Research, 178*(1), 339-345.

Moser, M., & Leo, O. (2010). Key concepts in immunology. *Vaccine, 28 Suppl 3*, C2-13.

Narimatsu, M., Maeda, H., Itoh, S., Atsumi, T., Ohtani, T., Nishida, K., et al. (2001). Tissue-specific autoregulation of the stat3 gene and its role in interleukin-6-induced survival signals in T cells. *Molecular and Cellular Biology, 21*(19), 6615-6625.

Navarro-Gonzalez, J. F., Mora-Fernandez, C., Muros de Fuentes, M., & Garcia-Perez, J. (2011). Inflammatory molecules and pathways in the pathogenesis of diabetic nephropathy. *Nature Reviews.Nephrology, 7*(6), 327-340.

Neish, A. S., Read, M. A., Thanos, D., Pine, R., Maniatis, T., & Collins, T. (1995). Endothelial interferon regulatory factor 1 cooperates with NF-kappa B as a transcriptional activator of vascular cell adhesion molecule 1. *Molecular and Cellular Biology, 15*(5), 2558-2569.

Paulson, M., Pisharody, S., Pan, L., Guadagno, S., Mui, A. L., & Levy, D. E. (1999). Stat protein transactivation domains recruit p300/CBP through widely divergent sequences. *The Journal of Biological Chemistry, 274*(36), 25343-25349.

Paun, A., & Pitha, P. M. (2007). The IRF family, revisited. *Biochimie, 89*(6-7), 744-753.

Pine, R. (1997). Convergence of TNFalpha and IFNgamma signalling pathways through synergistic induction of IRF-1/ISGF-2 is mediated by a composite GAS/kappaB promoter element. *Nucleic Acids Research, 25*(21), 4346-4354.

Rozen, S., & Skaletsky, H. (2000). Primer3 on the WWW for general users and for biologist programmers. *Methods in Molecular Biology (Clifton, N.J.), 132*, 365-386.

Savitsky, D., Tamura, T., Yanai, H., & Taniguchi, T. (2010). Regulation of immunity and oncogenesis by the IRF transcription factor family. *Cancer Immunology, Immunotherapy : CII, 59*(4), 489-510.

Schaefer, T. S., Sanders, L. K., Park, O. K., & Nathans, D. (1997). Functional differences between Stat3alpha and Stat3beta. *Molecular and Cellular Biology, 17*(9), 5307-5316.

Teglund, S., McKay, C., Schuetz, E., van Deursen, J. M., Stravopodis, D., Wang, D., et al. (1998). Stat5a and Stat5b proteins have essential and nonessential, or redundant, roles in cytokine responses. *Cell, 93*(5), 841-850.

Tervaert, T. W., Mooyaart, A. L., Amann, K., Cohen, A. H., Cook, H. T., Drachenberg, C. B., et al. (2010). Pathologic classification of diabetic nephropathy. *Journal of the American Society of Nephrology : JASN, 21*(4), 556-563.

Udy, G. B., Towers, R. P., Snell, R. G., Wilkins, R. J., Park, S. H., Ram, P. A., et al. (1997). Requirement of STAT5b for sexual dimorphism of body growth rates and

liver gene expression. *Proceedings of the National Academy of Sciences of the United States of America, 94*(14), 7239-7244.

Upton, G., & Cook, I. (2008). *A dictionary of statistics* Oxford University Press.

van Belle, T. L., Coppieters, K. T., & von Herrath, M. G. (2011). Type 1 diabetes: Etiology, immunology, and therapeutic strategies. *Physiological Reviews, 91*(1), 79-118.

Yanai, H., Negishi, H., & Taniguchi, T. (2012). The IRF family of transcription factors: Inception, impact and implications in oncogenesis. *Oncoimmunology, 1*(8), 1376-1386.

Yang, J., Chatterjee-Kishore, M., Staugaitis, S. M., Nguyen, H., Schlessinger, K., Levy, D. E., et al. (2005). Novel roles of unphosphorylated STAT3 in oncogenesis and transcriptional regulation. *Cancer Research, 65*(3), 939-947.

Yang, J., Liao, X., Agarwal, M. K., Barnes, L., Auron, P. E., & Stark, G. R. (2007). Unphosphorylated STAT3 accumulates in response to IL-6 and activates transcription by binding to NFkappaB. *Genes & Development, 21*(11), 1396-1408.

Ye, J., Coulouris, G., Zaretskaya, I., Cutcutache, I., Rozen, S., & Madden, T. L. (2012). Primer-BLAST: A tool to design target-specific primers for polymerase chain reaction. *BMC Bioinformatics, 13*, 134-2105-13-134.

Yue, H., Li, W., Desnoyer, R., & Karnik, S. S. (2010). Role of nuclear unphosphorylated STAT3 in angiotensin II type 1 receptor-induced cardiac hypertrophy. *Cardiovascular Research, 85*(1), 90-99.

Yu-Lee, L. (2001). Stimulation of interferon regulatory factor-1 by prolactin. *Lupus, 10*(10), 691-699.

Thesis and Dissertation Services